Master's Thesis of Pharmacy

Zeb2 repression during cellular reprogramming promotes metabolic transition and entry of pluripotency

세포 리프로그래밍 중 Zeb2 억제를 통한 대사 전환 및 다능성 진입 촉진

August 2022

Graduate School of Pharmacy
Seoul National University
Pharmaceutical Sciences Major

Ji-Young Oh

Zeb2 repression during cellular reprogramming promotes metabolic transition and entry of pluripotency

지도 교수 차 혁 진

이 논문을 약학석사 학위논문으로 제출함
2022 년 5 월

서울대학교 대학원
약학과 약학전공
오 지 영

오지영의 약학석사 학위논문을 인준함
2022 년 7 월

위 원 장 _____ 한 병 우 _____ (인)

부위원장 _____ 구 자 현 _____ (인)

위 원 _____ 차 혁 진 _____ (인)

Abstract

Metabolic transition to glycolysis that occurs in the cellular reprogramming has been demonstrated to be a prerequisite event for acquisition of pluripotency by determination of overall efficiency after genetic perturbations. Here, with ATP-Red1, a specific fluorescent probe for mitochondrial ATP and mouse embryonic fibroblasts (MEFs) harboring inducible reprogramming factors (i4F-MEF), we enabled to lively isolate the population with metabolic transition induced by reprogramming and performed the characterization. Consistently, ATP-Red1 low population (ATP-low), representing the metabolic transition to glycolysis, lively isolated in the middle of reprogramming, revealed the higher reprogramming capacity than ATP-Red1 high (ATP-high) population. Through transcriptome profile analysis between ATP-high and ATP-low, we also demonstrated that transcriptome from ATP-low was negatively correlated to epithelial mesenchymal transition (EMT) with clear repression of Zeb2, a master regulator of EMT. Of note, depletion of Zeb2 was solely sufficient to subside the level of mitochondrial ATP and improve the overall reprogramming efficiency. These results imply that elevation of epithelial trait from i4F-MEF via Zeb2 suppression, would lead to metabolic transition for facilitating cellular reprogramming.

Keyword: *Zeb2*, Reprogramming, EMT, Metabolic transition, ATP-Red 1, iPSC

Student Number: 2020-20464

Table of Contents

List of Figure

List of Table

Abbreviations

mESCs	mouse Embryonic Stem Cells
LIF	Leukemia Inhibitory Factor
2i	two inhibitors, Mek1 inhibitor and GSK3β inhibitor
iGsk3β	Gsk3β inhibitor, CHIR99021
iMek1	Mek1 inhibitor, PD0325901
MEF	Mouse Embryonic Fibroblast
OSKM	Oct4, Sox2, Klf4, c-Myc
OG2	Oct4-ΔPE-GFP cell
POG2	Primed- Oct4-ΔPE-GFP cell
GSEA	Gene set enrichment analysis
DMSO	Dimethyl sulfoxide
DMEM	Dulbecco's modified eagle medium
FBS	Fetal bovine serum
EMT	Epithelial Mesenchymal Transition
MET	Mesenchymal Epithelial Transition
iPSCs	induced Pluripotent Stem Cells
CDg4	compound of designation green 4
OxPHOS	Oxidative phosphorylation
FCCP	Carbonyl cyanide-p-trifluoromethoxyphenylhydrazone
2-DG	2-Deoxyglucose
OCR	Oxygen consumption rates

Introduction

Distinct metabolic profiles in naïve and primed pluripotency

Although both human and mouse embryonic stem cells (ESCs) are derived from the inner cell mass (ICM) of the blastocyst, the cellular and molecular characteristics of human embryonic stem cells (hESCs) differ from those of mESCs [1], which may account for differences in the early development of human and mouse embryos [2]. Two distinct pluripotency states have been distinguished, naïve (or ground) and primed, to characterize the status of pluripotent stem cells (PSCs) peri- and post-implantation [3]. Differences in pluripotency status (e.g., naïve vs. primed) account for many distinct features of hESCs, such as glucose metabolism [4], dissociation-induced cell death [5], poor genome-editing efficiency [6], and high dependency on the basic fibroblast growth factor 2 (Fgf2)/Akt signaling [7] instead of the leukemia inhibitor factor (Lif)/Stat3 signaling [8]. Gaining a better insight into the unique characteristics of naïve ESCs to undergo organogenesis in other embryos is a critical prerequisite for understanding the mechanisms of embryonic chimerism [i.e., a mixed organism with different cell populations derived from more than one embryo [9]]. The potential of chimera formation of naïve ESCs would be further applied for future regenerative medicine [10], in addition to contributing to the general understanding of early embryogenesis [11].

Considerable effort has been devoted to establishing an efficient protocol that can convert primed hESCs to naïve hESCs to derive the human counterparts of rodent naïve PSCs with long-term stability [12], [13]. However, the low primed-to-naïve conversion efficiency of hESCs and the unstable maintenance of their naïve

characteristics require additional processes to selectively isolate ESCs in a naïve-like state. Strategies that employ genetic tagging [14] or identification of surface antigens [15], [16] or fluorescence probes [17] specific to naïve hESCs have enabled live isolation of homogenous naïve populations for experimental purposes.

Whereas primed ESCs prefer glycolysis [4], naïve ESCs also use mitochondrial oxidative phosphorylation (OxPHOS) to produce ATP [18]. The metabolic shift that occurs in the transition between naïve and primed state is regulated by metabolites (e.g., 1-methylnicotinamide or α-ketoglutarate) to directly affect the epigenetic status produced from the different glucose metabolism [19], [20]. In particular, two chemical inhibitors (iGsk3β and iMek1, targeting Gsk3β and Mek1, respectively) along with Lif (hereafter Lif/2i) are critical for this metabolic conversion [20], [21]. The expression of Esrrb, a typical naïve-specific marker gene by inhibition of Gsk3β through Tcf3 derepression [22], promotes OxPHOS [23]. These studies suggest that Gsk3β activity is associated with the metabolic switch from the primed to the naïve state. It is also noteworthy that endogenous ligand, Netrin-1 and Netrin-1 receptor (e.g., Neo1 and Unc5B) signaling, inactivates Gsk3α/β in the pre-implantation embryo as well as in naïve ESCs [24], and this inactivation accounts for the gradual increase in intracellular glycogen level in the pre-implantation mouse embryo [25].

In this study, we demonstrate that the high glycogen level in naïve ESCs reacted with compound of designation green 4 (CDg4), a fluorescent probe for glycogen [26], and this probe was selective enough to isolate both mouse and human naïve ESCs from a mixture with primed ESCs. The distinct glucose metabolism, which relies on the inhibition of Gsk3β to activate glycogen synthase (Gys, encoded by Gys1), was responsible for the glycogen accumulation in naïve ESCs and their subsequent

tolerance to transient disruption of glycolysis, unlike primed ESCs. Thereby, enrichment of naïve ESCs was readily achieved by their exclusive glucose metabolism, suggesting that high intracellular glycogen accumulation can delineate the metabolic remodeling during the transition to naïve pluripotency.

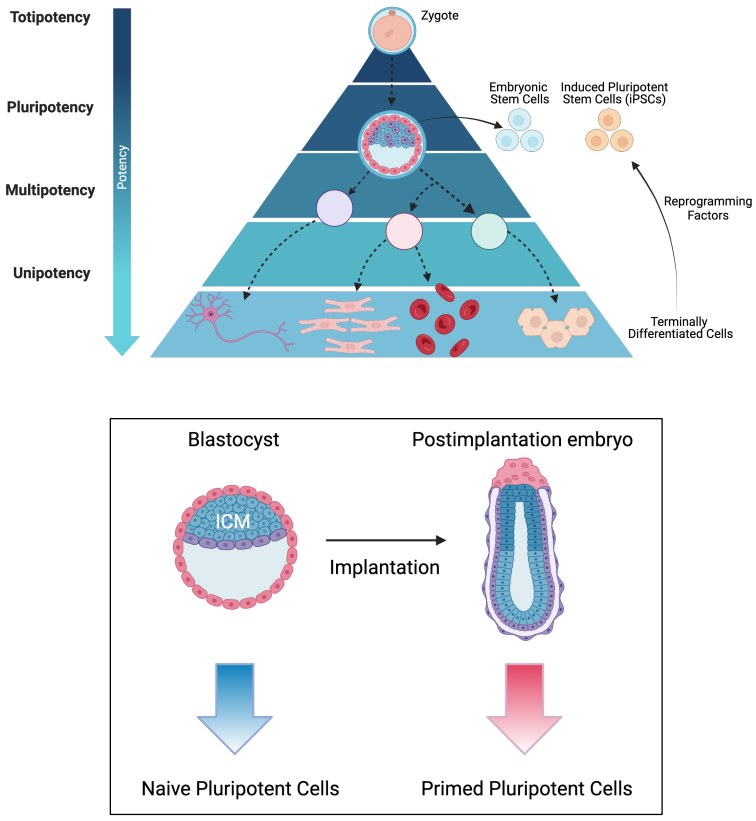

Figure 1. Naive and Primed pluripotency

Pluripotency has two distinct states, Naïve and primed pluripotency, which recapitulate the pluripotency before and after implantation.

Metabolic transition in reprogramming

Induced pluripotent stem cells (iPSCs) can be generated from somatic cells by introduction of defined transcription factors [27, 28]. Mesenchymal-to-epithelial transition (MET) occurs at an early stage of reprogramming [29, 30] and MET is characterized by upregulation of epithelial genes such as *E-Cadherin, Cdh1* and downregulation of mesenchymal genes such as *N-Cadherin, Snail1/2* and *Zeb1/2* [31]. Although iPSC technology has been considered as an invaluable resource in various clinical/research studies [32], this approach carries significant limitations, such as poor reprogramming efficiency and slow dynamics brought on by the presence of strong barriers [33, 34]. Epigenetic barrier and reprogramming-induced stress barrier are representative, and many attempts have been made to increase reprogramming efficiency by removing these barriers [35-37].

It is well known that somatic cells undergo metabolic transition during cellular reprogramming [38, 39] and metabolic control can regulate stem cell function [4]. However, the exact reasons why this metabolic transition occur and how metabolism is linked to pluripotency have not yet been fully elucidated. In this study, we demonstrate that ATP level based on distinct metabolic profiles can determine reprogramming efficiency using ATP-Red 1, a fluorescent probe for mitochondrial-ATP [40], and this probe was able to capture compare groups that undergo metabolic transition during reprogramming. Thereby, our study unravels the potential of metabolic barriers in cellular reprogramming.

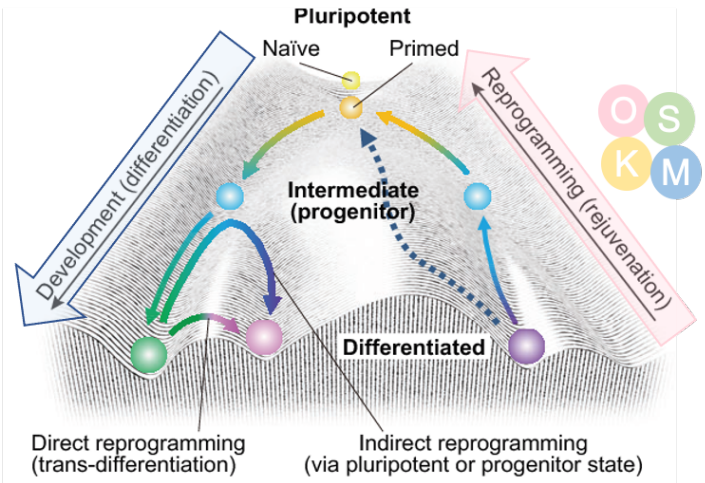

Adapted from Takahashi et al., development, 2015

Figure 2. Development and reprogramming

Pluripotent stem cells can differentiate into any somatic lineage, not only during development but also in response to extrinsic cues in vitro. Induced pluripotent stem cells (iPSCs) can be generated by converting somatic cells to a pluripotent state using a combination of OSKM expression and optimal conditions.

Materials and Methods

1. Cell culture

Naïve mouse ESCs (mESCs) and induced pluripotent stem cells (iPSCs) were cultured on 0.5% gelatin-coated dish in Naïve mESC culture media [DMEM high glucose (Gibco) supplemented with 15% FBS (Gibco), 1% MEM-nonessential amino acids (Gibco), 1% Glutamax (Gibco), 0.1 mM β-mercaptoethanol (Gibco), 0.1% Gentamycin (Gibco), 1,000 U/ml mouse leukemia inhibitory factor (mLIF) (Millipore, Merk), 3 μM Gsk3 inhibitor CHIR99021 (Peprotech) and 1 μM MEK inhibitor PD0325901 (Peprotech)] at 37°C and 5% CO_2 condition. Cells were passaged 1:5-1:10 every 2-3 days using 0.25% Trypsin/EDTA (Wellgene).

Primed mouse ESCs were culture on Matrigel (Corning# 354377)-coated dish with EpiSC culture media [DMEM/F12 (Gibco) supplemented with 15% KOSR (Gibco), 1% MEM-nonessential amino acids (Gibco), 1% Glutamax (Gibco), 0.1% Gentamycin (Gibco), 10 ng/ml murine bFgf (Peprotech), 20 ng/ml murine Activin-A (Peprotech)] at 37°C and 5% CO_2 condition. Primed mESCs were weekly sub-cultured. 1 U/ml of Dispase (Gibco) solution was used for colony detachment. Colony clumps were dissociated and transferred 1:10-1:20 ratio on Matrigel (Corning# 354277) coated dishes. Culture media was daily changed for all cell types.

Mouse embryonic fibroblasts (MEFs) were cultured in MEF medium [DMEM (Hyclone) supplemented with 10% FBS (Corning), 0.1% Gentamycin (Gibco)] at 37°C and 5% CO_2 condition.

2. Glycogen quantification assay

Cellular glycogen amounts were determined by using colorimetric glycogen assay kit (BioVision) following manufacturer's instruction. For the sample preparation, cells were washed with DPBS for twice and single cell dissociated using Accutase (Sigma) solution. 1 million cells were counted and homogenized with cold distilled water for 1 hr in ice. Then lysates were boiled for 10 mins and supernatants were collected after centrifugation at 13,000 rpm 4 ^{o}C for 20 mins. Optical density for glycogen products was measured at 570 nm using Epoch microplate spectrophotometer (BioTek). Final glycogen concentration was normalized to initial protein input of each sample.

3. Fluorescent probe staining and flowcytometric analysis

For live staining of CDg4, the probe was diluted to final concentration as 3 μM in culture media and incubated for 1hr at 37°C. For staining after fixation and permeabilization, cells were fixed with 4% PFA (paraformaldehyde) for 10 mins at room temperature and treated with 0.1% TBS-T for 5 mins for permeabilization. 3 μM of CDg4 was treated to the fixed cell afterward. For flowcytometric analysis, cells were dissociated into single-cell using Trypsin/EDTA (Wellgene) or Accutase solution (Sigma) and inactivated with DMEM (Gibco) supplemented with 10% FBS (Gibco) or diluted in DPBS, respectively. For ATP-Red1 staining, identical number of suspended cells were stained with 2.5 mM of ATP-Red1 for 30 mins in 37°C. ATP-Red1 staining was terminated by adding PBS buffer into the suspended cells. Stained cells were collected in 5ml round-bottom tubes (Falcon) after strain and analyzed using FACSAria^{TM} (BD Bioscience) or FACSCalibur^{TM} (BD Bioscience). Data were analyzed by FlowJo Software.

4. RNA isolation and quantitative RT-PCR analysis

Total RNA was extracted from cells using Easy-Blue™ total RNA isolation kit (iNtRON Biotech) followed by the supplier's instruction. PrimeScript™ RT reagent kit (TaKaRa) was used to generate cDNA and quantitative real-time PCR was performed using TB-Green PCR reagent (TaKaRa) by LightCycler-480®II (Roche). *Rn18s* or *Actb* genes were used as internal controls for normalizing gene expression data.

5. Derivation of MEFs

Mouse embryonic fibroblasts (MEFs) were isolated from embryos obtained from 13.5 day pregnant R26rtTA;Col1a14F2A mice (Jackson Laboratory #011004). After the head, tail, limbs and internal organs were removed, the remaining regions were subsequently washed with DPBS, minced into small pieces with scissors and digested with 0.25% Trypsin/EDTA (Wellgene) in a 37ºC for 10 min. After trypsinization, an equal volume of MEF medium was added and the cells were dissociated by pipetting up and down. The cells were centrifuged at 1000 rpm for 3 minutes and then resuspended in MEF medium. A total of 1×10^6 cells per 100mm dish were cultured and marked as passage 0. MEFs were used within three passages.

6. Cell Reprogramming

For reprogramming, MEFs were plated on 0.5% gelatin-coated dish in MEF medium. From the next day, cells were cultured in MEF medium supplemented with doxycycline (2μg/ml) for 3 days. Cells were then fed with Naïve mESC culture media supplemented with doxycycline (2μg/ml) daily for indicated periods. After

2~3 weeks, colonies were picked or stained for further analysis.

7. Spontaneous Differentiation

iPSCs underwent spontaneous differentiation through the formation of embryoid bodies (EBs) in basal medium, following the removal of growth factors and small molecules. The expression levels of ectodermal, endodermal and mesodermal marker were compared relative to the expression of *Rn18s* gene in each sample.

8. Teratoma formation assay

1 x 10^6 cells of iPSCs were injected intramuscularly, intratesticularly and subcutaneously into 6-week-old male BALB/C nude mice. Teratomas were allowed to form for 6 weeks, and subsequently dissected and fixed with 4% PFA (paraformaldehyde) prior to histological analysis by hematoxylin and eosin (H&E), Masson's trichrome and Alcian Blue staining. These animal experiments were conducted under the permission of Seoul National University Institutional Animal Care and Use Committee (Permission number: SNU-210326-5-4).

9. Metabolic flux assays

To profile cellular metabolism, oxygen consumption rates (OCR) was measured using Seahorse XFe96 Analyzer (Agilent). For cell preparation, 5×10^4 cells were seeded in each well coated with 0.5% gelatin 1 day before the measurement. To prepare inhibitors for OCR measurement, 100 μM of oligomycin, 100 μM FCCP and 50 μM Rotenone/Antimycin (R/A) were diluted using Seahorse XF Cell Mito Stress Test Kit (Agilent#103015-100) and loaded in Sensor Cartridge (Agilent). Final

compound concentration for this experiment was 1 μM of oligomycin, 1 μM FCCP and 0.5 μM Rotenone/Antimycin (R/A). Measurement and analysis of each parameters followed the manufacturer's instruction (Seahorse XFe96 Analyzer, Agilent). OCR value was normalized with cell numbers exactly counted after nucleus counter-staining with Hoechst 33342 at the final step of the assay.

10. Alkaline phosphatase assay

Alkaline phosphatase (AP) staining was performed using AP staining kit (Sigma-Aldrich #86R-1KT) to visualize cell reprogramming. Overall procedure was followed by the manufacturer's instructions.

11. Transcriptome Analysis

For analysis of reprogrammed MEFs, total RNA was isolated using Easy-BLUE™ RNA isolation kit (iNtRON Biotechnology). RNA purity was determined by assaying 1 μl of total RNA extract on a NanoDrop8000 spectrophotometer. Total RNA integrity was checked using an Agilent Technologies 2100 Bioanalyzer with an RNA Integrity Number (RIN) value. mrna sequencing libraries were prepared according to the manufacturer's instructions (Illumina Truseq stranded mRNA library prep kit). MRNA was purified and fragmented from total RNA (1ug) using poly-T oligo-attached magnetic beads using two rounds of purification. Cleaved RNA Fragments primed with random hexamers were reverse transcribed into first strand cDNA using reverse transcriptase, random primers, dUTP in place of dTTP. (The incorporation of dUTP quenches the second strand during amplification, because the polymerase does not incorporate past this nucleotide.) These cDNA

fragments then had the addition of a single 'A' base and subsequent ligation of the adapter. The products were purified and enriched with PCR to create the final strand specific cDNA library. The quality of the amplified libraries was verified by capillary electrophoresis (Bioanalyzer, Agilent). After qPCR using SYBR Green PCR Master Mix (Applied Biosystems), we combined libraries that index tagged in equimolar amounts in the pool. Cluster generation occurred in the flow cell on the cBot automated cluster generation system (illumina). And then the flow cell loaded on Novaseq 6000 sequencing system (Illumina), performed sequencing with 2x100bp read length.

FPKM values of RNA sequencing data were formatted and loaded to run Gene Set Enrichment Analysis. And we used Enrichr's web-based tools and services to analyze Gene ontology terms significantly enriched in the various gene sets.

12. RNA interference

For knockdown of *Zeb2* during reprogramming, siRNA (Bioneer) against Zeb2 was transfected into MEFs by using DharmaFECT™ (Dharmacon). The siRNA sequences used in this study are listed in Table 2. For a stable knockdown of *Zeb2* during reprogramming, MEFs were infected with shRNA Lentiviral particles (Santa Cruz Biotechnology #sc-38642-V) according to the protocol of the manufacturer. MOI (Multiplicity of Infection) of 2 was used in this study.

13. Generation of TP53 Knockout iPSCs using CRISPR

p3s-Cas9-HN (addgene no.104171) and sgRNA were transfected to iPSCs using Lipofectamine 3000 (Invitrogen) according to the protocol of the manufacturer.

Pools of clones were screened by T7E1 assay and single colony selection was performed from heterogenous Trp53 KO pool cells. sgRNA sequences and T7E1 primer information are listed in Table 3 and 4.

14. Statistical analysis

The quantitative data are expressed as the mean values ± standard deviation (SD). Unpaired two-tailed *t*-tests was performed to analyze the statistical significance of each response variable. Pre-specified comparisons between groups were conducted (when appropriate) by Tukey's post hoc test using the PRISM. *p*-values less than 0.05 were considered statistically significant (* < 0.05, ** <0.01, ***<0.001, ****<0.0001 and n.s. for not significant).

Table1. Primer sequences for RT-qPCR

Primer Pairs for RT-qPCR		Primer Sequences (5'-3')
Nrob1	F	ACAGAGCAGCCACAGATGGTGTC
	R	GATGTGCTCAGTAAGGATCTGCTG
Dppa3	F	CGTACCTGTGGAGAACAAGAGTG
	R	CATTCTCAGAGGGATCCCATCTTTG
Esrrb	F	GATTCTCATCTTGGGCATCGTGTAC
	R	CTGACTCAGCTCATAGTCCTGCAG
T	F	CATCTGCTTGTCTGTCCATGCTG
	R	GAGAACCAGAAGACGAGGACGTG
Eomes	F	CTCAGAGACACAGTTCATCGCTGTG
	R	CAGGGACAATCTGATGGGATCTAGG
Fgf5	F	CATCGGTTTCCATCTGCAGATCTAC
	R	GTTCTGTGGATCGCGGACGCATAG
Cer1	F	GTGGAAAGCGATCATGTCTCATCG
	R	GCAAAGGTTGTTCTGGACAACGAC
Nanog	F	GTGCACTCAAGGACAGGTTTCAG
	R	CTGCAATGGATGCTGGGATACTC
Otx2	F	TCATGAGGGAAGAGGTGGCACTG
	R	AGCACTGCTGCTGGCAATGGTTG
Sox17	F	ACCCAGATCTGCACAACGCAGAG
	R	GCTTCATGCGCTTCACCTGCTTG
Zeb1	F	TGGAGTTCAAAGGTTGTCGTT
	R	TTGCCACATCAACACTGGTC
Zeb2	F	TTGCTCCAGGATGTGTGG
	R	CACACACTTGTTTGTGTGCATATC
Pou5f1	F	GAGAAAGCGAACTAGCATTGAGAAC
	R	TGTAGCCTCATACTCTTCTCGTTG
Sox2	F	ATGGGCTCTGTGGTCAAGTC
	R	CCCTCCCAATTCCCTTGTAT
Klf4	F	GAACAGCCACCCACACTTGTGAC
	R	CTGTCACACTTCTGGCACTGAAAG
c-Myc	F	ACCACCAGCAGCGACTCTGA
	R	TGCCTCTTCTCCACAGACACC
Twist2	F	CAG TGA CTT CTG TGC CCT CA
	R	TGA GAG CCT TGG TCC AGT TT
Col1A1	F	ACAAAACCCCTCGATAGAAGTGA
	R	CTCAGGTGCATACTCATCAATGT
Col1A2	F	TGGTCTTACTGGGAACTTTGCTGC
	R	ACCCTGTGGTCCAACGACTCCTCTC
Cdh2	F	AGGGTGGACGTCATTGTAGC
	R	CTGTTGGGGTCTGTCAGGAT

Table2. siRNA sequence information

Gene	siRNA sequence (5’ to 3’)
Zeb2	CAC UAG ACU UCA AUG ACU A=tt(1-AS)
	UAG UCA UUG AAG UCU AGU G=tt(1-AA)

Table3. T7E1 primer information

Primer Pairs for T7E1 assay		Primer Sequences (5'-3')
*Trp53*_1st PCR	F	CCA TCT TGG GTC CTG ACT TC
	R	TGG CCG ACT TCT TGG ATA CT
*Trp53*_2nd PCR	F	CAA AGC CCA AGT CCC TTT CT
	R	CCA AGT CCC TTT CTG CTC TG

Table4. sgRNA sequence information

Gene	gRNA sequence
Trp53	CCTCGAGCTCCCTCTGAGCCAGG

Results

Selective reactivity of CDg4, a fluorescence glycogen sensor, to naïve mESCs

To screen the naïve specific fluorescence probe, we took advantage of two isogenic pairs of naïve and primed mouse ESCs (mESCs) (e.g., naïve/primed: J1/P-J1 and OG2/P-OG2 respectively) in which typical markers of the naïve and primed states were evident. A set of naïve and primed mESCs was screened with 46 in-house fluorescent probes based on the DOFLA (Diversity Oriented Fluorescence Library Approach) (Fig. 3A), as described previously [41]. As a positive control, we used the CDy9 fluorescent probe, which selectively stains naïve mESCs [17].

Similar to the naïve-specific CDy9, another probe, CDg4, emerged from the screen as a highly specific marker of naïve mESCs (Fig. 3B). The specificity of CDg4 for naïve mESCs compared to primed mESCs (Fig. 3C) was highlighted by clear segregation of CDg4 signal in the mixture with primed ESCs. Dose-dependency experiments also supported the high specificity of CDg4 for naïve mESCs (Fig. 3D). CDg4 was previously reported to interact with glycogen in mESCs [26], and to bind stored glycogen in cancer cells [42]. To interrogate the binding specificity of CDg4, we examined the reactivity of a pair of naïve and primed mESCs to CDg4 with or without cell fixation, which allows the free cellular entry of the fluorescence probe due to abrogation of the selective membrane permeability. Consistent with previous reports [26, 42], the CDg4 fluorescent signal in the live naïve mESCs was localized to the cell surface without cell fixation. On the other hand, naïve specific CDg4 signal was evident from inside of the cells after fixation (Fig. 3E). Of note, the cell type specificity of fluorescence probe is designated as

either ‘holding-oriented’ (i.e., from the presence of specific holding target for probe) or ‘gating-oriented’ (i.e., from the presence of specific membrane transporter for probe) mechanism [43]. Accordingly, the high CDg4 signal from naïve mESCs regardless of cell fixation implies that naïve specific CDg4 reactivity would be ‘holding-oriented’ but not ‘gating-oriented’. Thus, we presumed that glycogen, a known holding target for CDg4 [26], would be higher in naïve than primed ESCs.

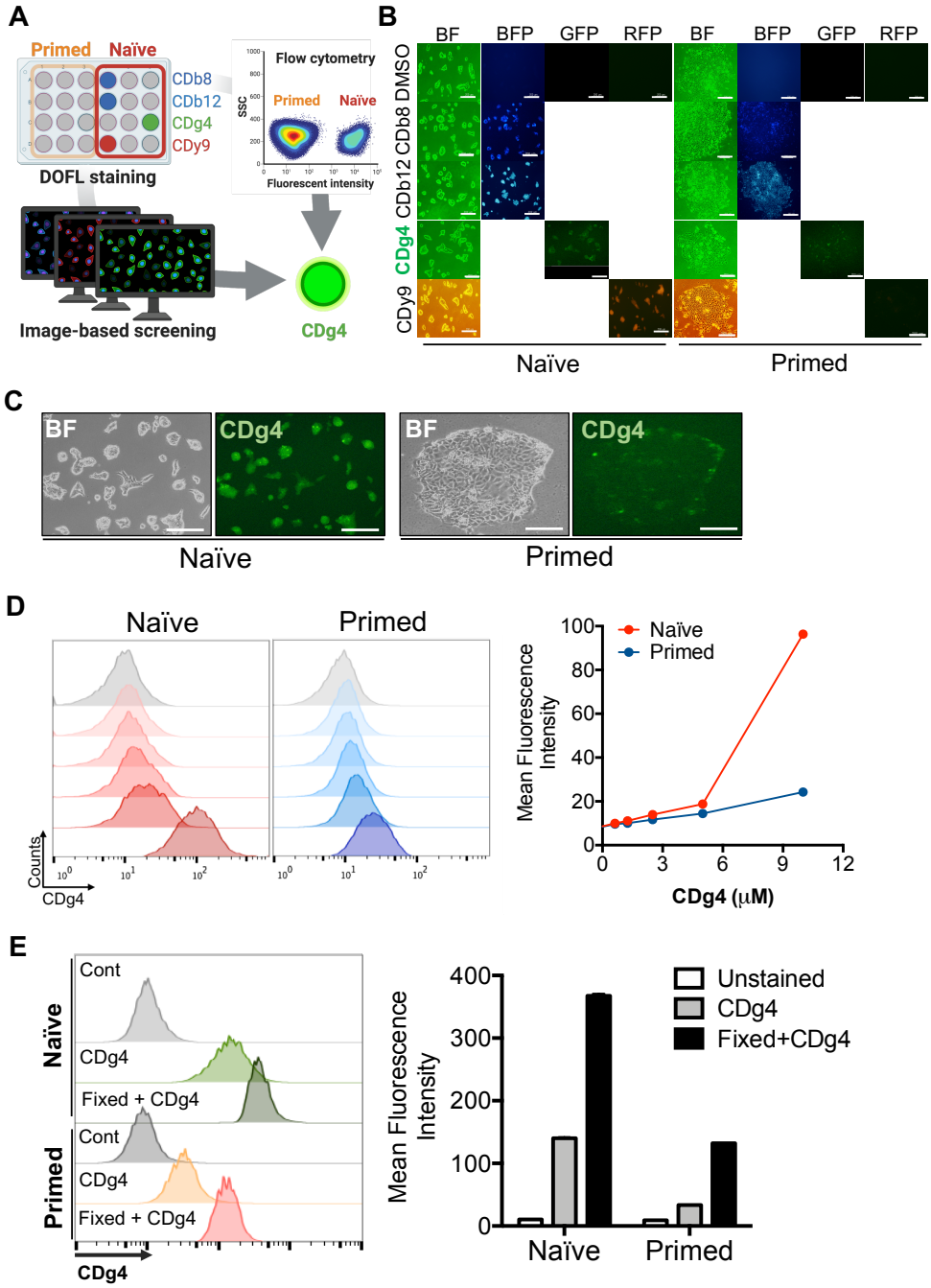

Figure 3. Selective reactivity of CDg4, a fluorescence glycogen sensor, to naïve mESCs (A) Graphical summary for screening fluorescent probes with high selectivity toward naïve mESCs (B) Phase contrast and fluorescent microscope images of J1 naïve and PJ1 primed mESCs after fluorescent probes (CDb8, CDb12,

CDg4, CDy9) staining. Scale bars, 200 μm. (C) Phase contrast and fluorescent microscope images of J1 naïve and PJ1 primed mESCs after CDg4 staining. Scale bars, 200 μm. (D) Relative fluorescent intensity of naïve and primed mESCs after CDg4 treatment with indicated concentrations. Mean fluorescent intensity was determined and presented as graph (right panel). (E) Relative fluorescent intensity of J1 naïve and PJ1 primed mESCs stained with CDg4 was determined before and after cell fixation with 4% paraformaldehyde. Mean fluorescent intensity of CDg4 was determined as graph (right panel).

Distinct intracellular glycogen storage in naïve mESCs

As expected, intracellular glycogen was significantly elevated in two independent pairs of naïve mESCs compared to primed mESCs (Fig. 4A). It has been well documented that constant inhibition of Gsk3β is critical for not only maintaining but also achieving naïve pluripotency [44] to promote Wnt/β-catenin signaling through β-catenin stabilization. Besides, Gsk3β directly phosphorylates and inhibits glycogen synthases (encoded by *Gys1*). Thus, a constant supplement of iGsk3β (CHIR99021: CHIR) in naïve ESCs may induce glycogen synthesis, which attributes to the high reactivity of CDg4. (Fig. 4B)

To examine the effect of iGsk3β, naïve or primed mESCs were maintained with or without iGsk3β. While we observed a drastic reduction in intracellular glycogen level in naïve mESCs in the absence of iGsk3β, the level of glycogen in primed mESCs remained minimal with or without iGsk3β treatment (Fig. 4C). Similarly, glycogen in NIH3T3 cells remained low even after iGsk3β treatment, while marked reduction of glycogen in the naïve state occurred after withdrawal of iGsk3β (Fig. 4D). We concluded that the naïve specificity of CDg4 is due to elevated glycogen synthesis upon Gsk3β inhibition and this metabolic difference is a unique feature of naïve mESCs that distinguishes them from primed ESCs.

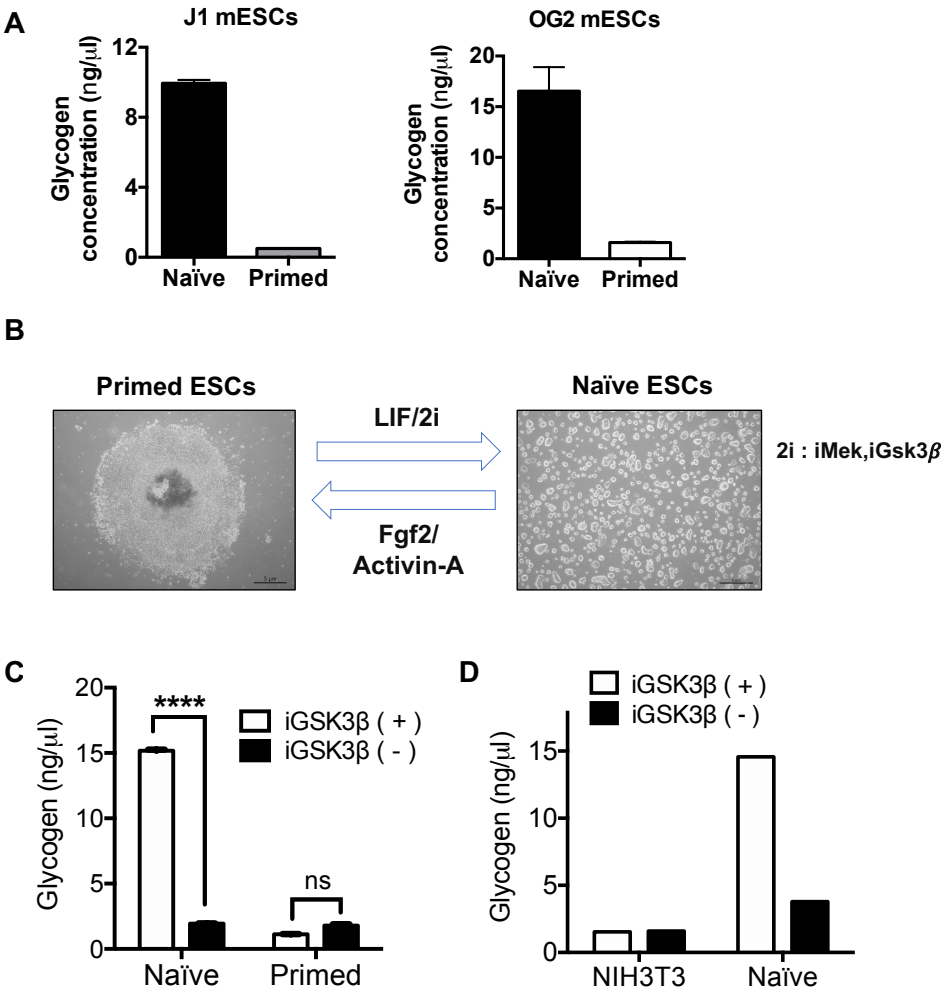

Figure 4. Distinct intracellular glycogen storage in naïve mESCs (A) Determination of glycogen contents in isogenic naïve and primed pair of J1 and OG2 mESCs. (B) Different culture condition between navie and primed ESCs. Intracellular glycogen amounts were determined between J1 and PJ1 mESCs (C), between NIH3T3 cells and naïve mESCs (D) in the presence or absence of iGsk3β for 30 hrs (n=3 independent experiments, **** p<0.0001, ns indicates significant, unpaired t-test for statistical analysis).

Live isolation of naïve mESCs by CDg4 reactivity due to high glycogen level

Due to the low efficiency of conversion from primed (or epiblast) ESCs to naïve mESCs, live isolation (or enrichment) of naïve mESCs could be useful for efficiently establishing naïve mESCs. Thus, we next examined whether the high specificity of CDg4 toward naïve mESCs due to glycogen storage would be sufficient to enrich naïve mESCs in the middle of conversion from primed mESCs. To this end, the CDg4-positive population was isolated from a mixture of naïve and primed mESCs (Fig. 5A). After CDg4 was applied to a mixture of naïve and primed mESCs, cells within the upper 5% and lower 5% of the distribution of quantified CDg4 reactivity were isolated and maintained (Fig. 5B, left). As predicted, the cells obtained from the CDg4 positive population [CDg4(+)] showed the typical dome-shaped colony morphology of naïve mESCs, while cells sampled from the CDg4 negative population [CDg4(-)] displayed a flat colony morphology (Fig. 5B, right). Cellular characteristics of CDg4(+) and CDg4(-) populations were determined by specific marker expression levels. As expected, typical naïve markers were significantly increased in the CDg4(+) population (Fig. 5C), whereas the typical primed markers were highly expressed in the CDg4(-) population (Fig. 5D). It is noteworthy that the CDg4(+) and CDg4(-) populations showed higher levels of naïve and primed-specific marker expression respectively (Fig. 5C and D), implying that the specificity of CDg4 would be sufficient for live enrichment of naïve mESCs.

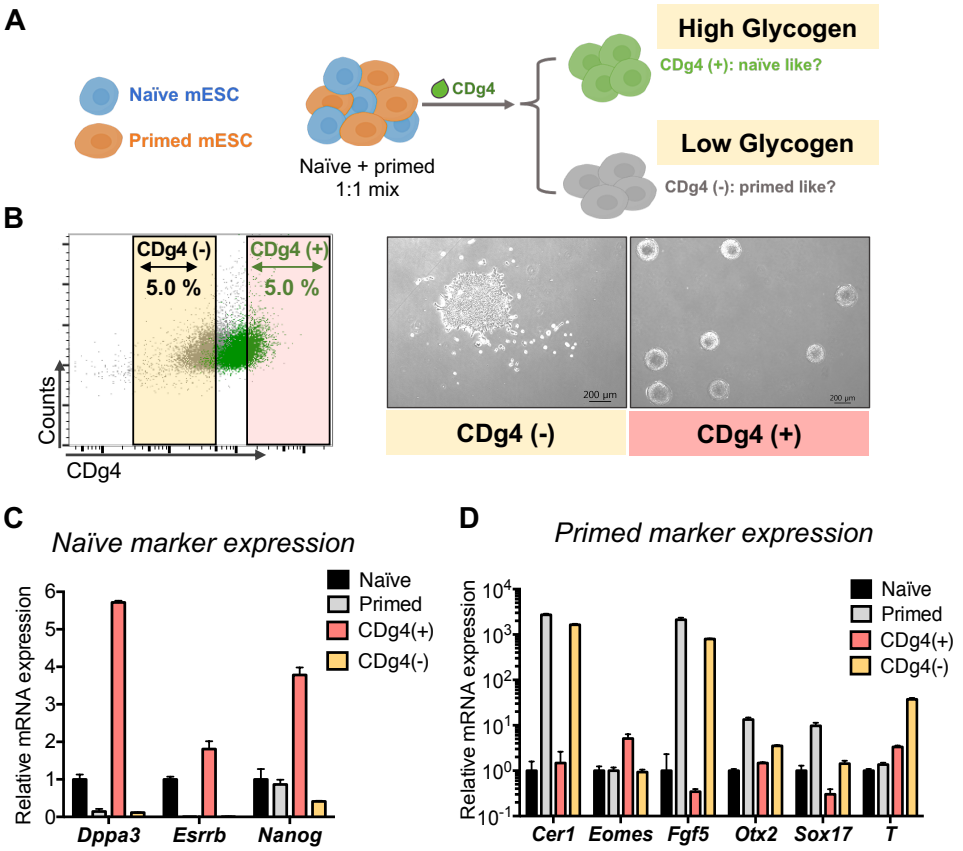

Figure 5. Live isolation of naïve mESCs by CDg4 reactivity due to high glycogen level (A) Graphical scheme of isolating CDg4 positive (CDg4+) and negative (CDg4-) population after staining CDg4 in naïve and primed mixed condition. Identical cell number of naïve and primed cells were mixed for staining. (B) Upper and lower 5.0% populations of CDg4 stained cells in Fig. 5A were isolated (left panel). Microscopic images of typical morphologies of CDg4(-) or CDg4 (+) populations. Scale bars, 200 μm. (C) Relative gene expression of naïve pluripotency markers (*Dppa3, Esrrb, Nanog*) and (D) primed specific markers (*Cer1, Eomes, Fgf5, Otx2, Sox17, T*) were determined in CDg4 (-) and CDg4 (+) populations compared with those of naïve and primed mESCs.

Live isolation of naïve mESCs by ATP-Red 1 reactivity due to high OxPHOS

Distinct metabolic profiles between naïve and primed mESCs have been well-characterized as naïve ESCs use OxPHOS and glycolysis bivalently to produce energy [45], in contrast with the exclusive glycolytic metabolism of primed mESCs for energy production [4, 18]. Considering glucose is a basic unit composing glycogen, we wondered whether skewed storage of intracellular glycogen in naïve mESCs resulted from the distinct glucose metabolism. We examined the effect of the perturbation on ATP production through either glycolysis or OxPHOS in naïve and primed mESCs. To this end, the intensity of a fluorescent probe for mitochondrial-ATP (ATP-Red1) [40] was monitored after metabolic perturbation with 2-Deoxyglucose (2-DG) [for glycolysis inhibition] or Carbonyl cyanide-p-trifluoromethoxyphenylhydrazone (FCCP) [for OxPHOS inhibition]. Overall ATP-Red1 intensity, high in naïve mESCs, was only markedly diminished by FCCP while that of primed mESCs was exclusively affected by 2-DG treatment (Fig. 6A). These results demonstrate that naïve and primed mESCs have distinct metabolic profiles. Furthermore, this distinctive labeling of ATP-Red1 between naïve and primed mESC enables isolation of ATP-Red1–high (upper 7%), –middle (7% covering median population), and –low (bottom 7%) populations in the mixture of naïve and primed mESCs (Fig. 6B and C). The typical dome-shaped morphology of naïve mESCs (indicated by yellow arrows, Fig. 6D) and naïve-specific gene expression (Fig. 6E) were increased in ATP-Red1–high population, suggesting that naïve mESCs were efficiently enriched based on the distinctive metabolic profiles of naïve mESCs.

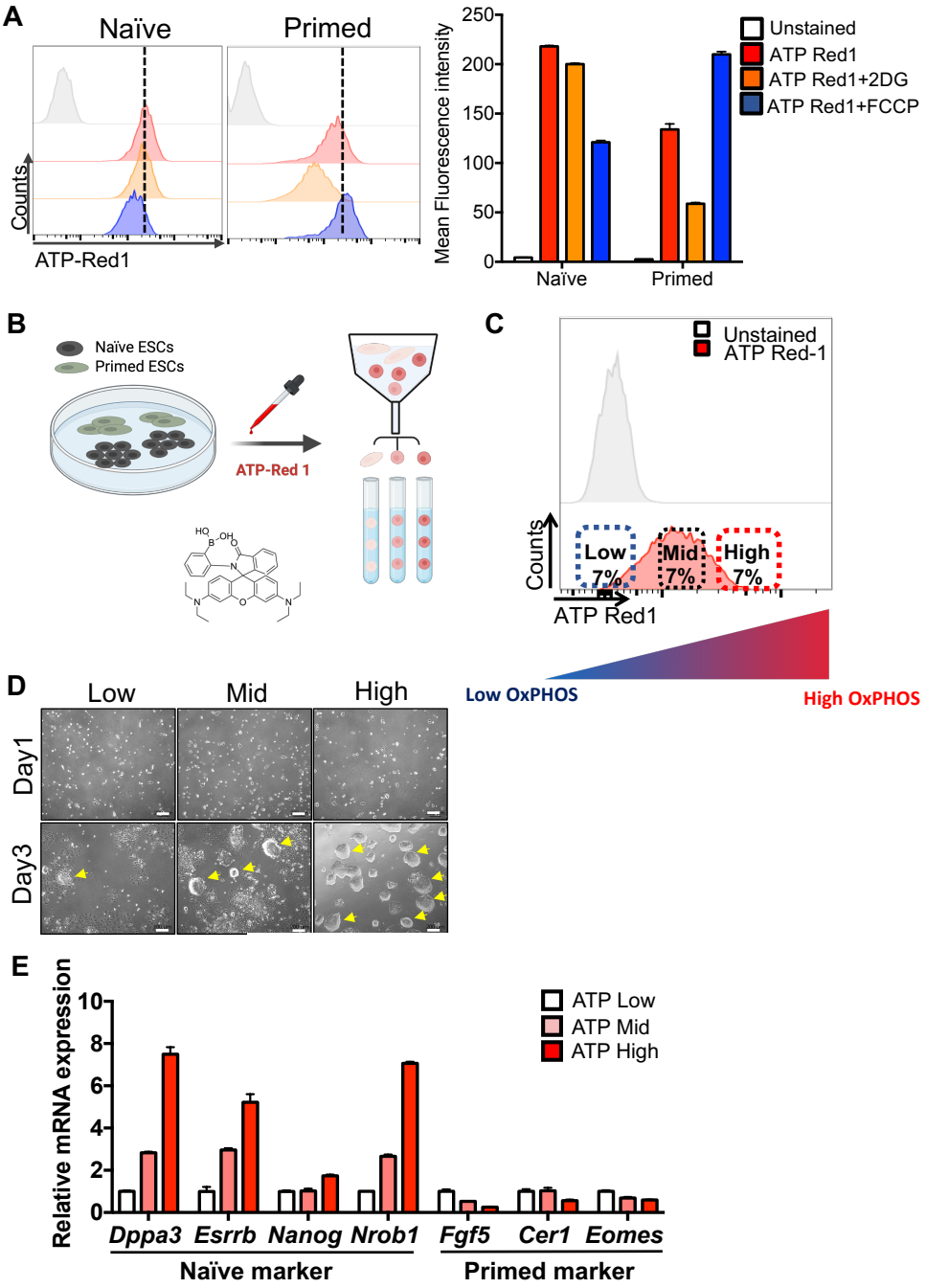

Figure 6. Live isolation of naïve mESCs by ATP-Red 1 reactivity due to high OxPHOS (A) Relative fluorescent intensity of naïve and primed mESCs stained with ATP-Red 1 (2.5μM, 30min), fluorescent probe detecting mitochondrial ATP levels with/without 2-DG (20mM, 12h), FCCP (5μM, 30min). Mean fluorescent

intensity of ATP-Red 1 was determined as graph in right panel (n=4 independent experiments). (B, C) Flowcytometric analysis of the intensity of ATP-Red1 and isolation of ATP-Red1 low/mid/high 7% population after staining with the probe in naïve and primed mixed condition. (D) Each upper, middle and lower 7% population in Fig. 6C were isolated and cultured for 3 days under naïve culture condition. Typical dome-shaped morphologies of naïve mESCs (yellow arrows) were enriched in ATP high population. Scale bars, 200 μm. (E) The relative gene expression of naïve pluripotency markers and primed specific markers in ATP-Red1 low/mid/high 7% populations right after sorting (n=3 biological replicates with n=2 independent experiments).

Establishment of inducible reprogramming cell model

So far, our results indicated that the high intracellular glycogen and the active OxPHOS as a novel biomarker delineating metabolic remodeling during the transition of naïve pluripotency[46]. However, considering the drastic metabolic transition occurring during early embryo development, it is also possible that the metabolic transition would serve as a certain role during cellular reprogramming, which occurs in the opposite direction. To examine this possibility, we took advantage of iPSC technology that the introduction of four specific genes encoding transcription factors (Oct4, Sox2, Klf4 and c-Myc, OSKM) could convert somatic cells into pluripotent stem cells [27]. In order to examine the role of metabolism in TF-induced cell reprogramming, we first derived embryonic fibroblasts (MEFs) from transgenic mouse strain (Fig. 7A) expressing the polycistronic 4F2A cassette (four mouse reprogramming genes Oct4 [Pou5f1], Sox2, Klf4, and c-Myc [Myc]) [47, 48]. Simple doxycycline treatment to induce these reprogramming factors allows somatic cells to be directly reprogrammed to generate iPSCs by culture. Upon reprogramming, MEFs gradually clustered and proliferated to form compact iPS-like colonies and exhibited elevated reprogramming factors (*Pou5f1, Sox2, Klf4 and c-Myc*) (Fig. 7B). We selected two clones (#1 and #2) of iPSCs and RT-qPCR analyses showed that both iPSCs revealed markedly increased endogenous reprograming factors as well as characteristic of naive ESCs, including *Esrrb* and *Nanog,* compared to MEF (Fig. 7C). To determine the in-vitro pluripotency of the iPSCs, tri-lineage differentiation was performed using the embryoid body (EB) protocol. We observed that iPSCs had the capacity to differentiate into cell types of ectoderm (*Otx2*), mesoderm (*Twist2*) and endoderm (*Sox17*) (Fig. 7D). Also, we evaluated the pluripotency of iPSCs by a teratoma formation assay. Following intratesticular,

subcutaneous and intramuscular injection in immunocompromised mice, derived iPSCs were capable of forming teratomas. As shown in Fig. 7E, the teratoma comprised derivatives from the three germ layers, including neuronal rosettes and keratin pearls (ectoderm); cartilage, and connective tissue (mesoderm); and, glands and ciliated epithelium (endoderm). Taken together, our data suggest that generated iPSCs from MEFs retain pluripotency and thus i4F-MEF model is adequate to examine the relevance of metabolism during reprogramming.

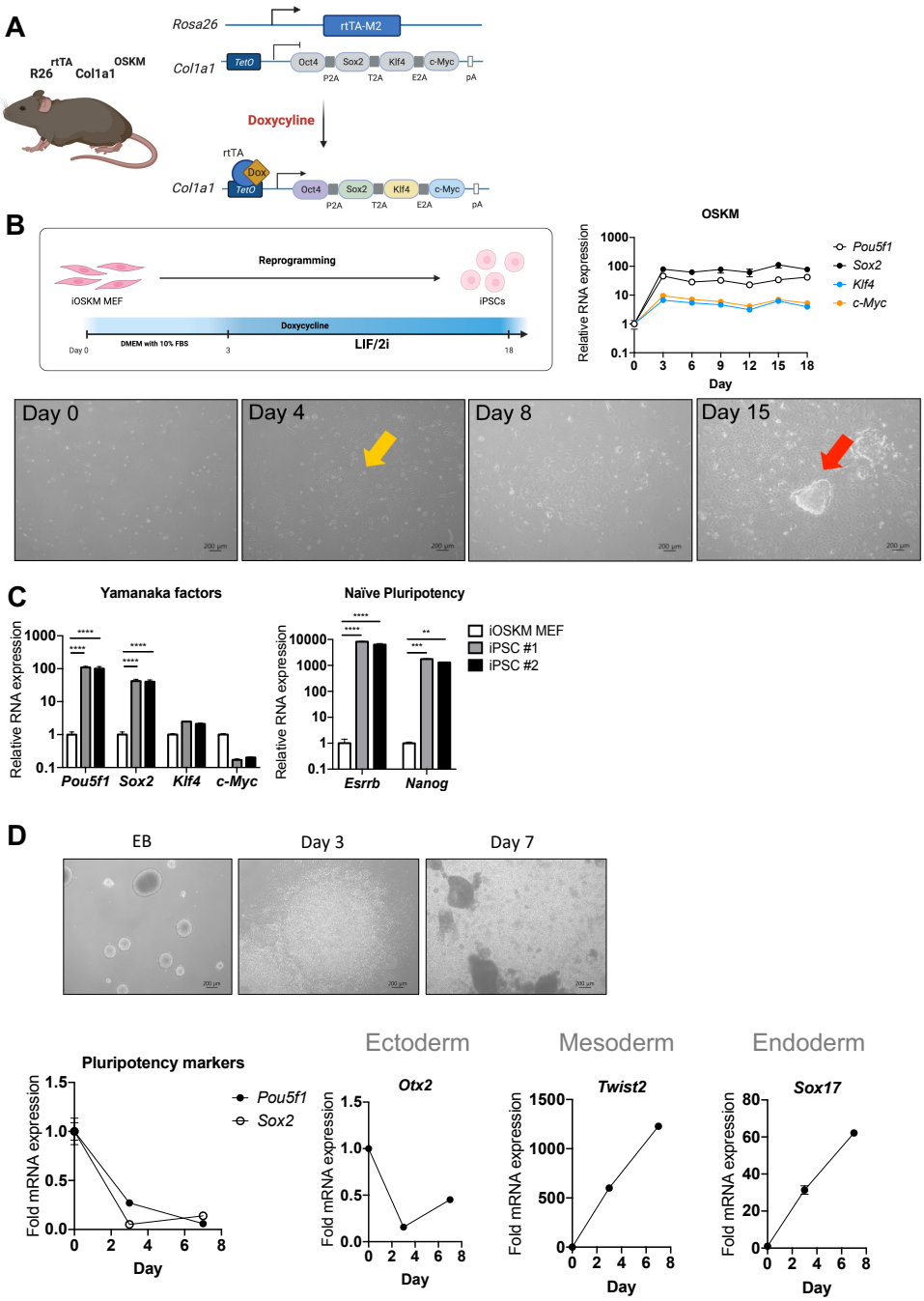
A
Rosa26
rtTA-M2
rtTA
OSKM
R26
Col1a1
Col1a1
TetO
Oct4
Sox2
Klf4
c-Myc
P2A
T2A
E2A
pA
Doxycyline
rtTA
Dox
B
Reprogramming
iOSKM MEF
iPSCs
Doxycycline
DMEM with 10% FBS
LIF/2i
Day 0
3
18
OSKM
Relative RNA expression
Pou5f1
Sox2
Klf4
c-Myc
Day
Day 0
Day 4
Day 8
Day 15
C
Yamanaka factors
Naïve Pluripotency
Relative RNA expression
Pou5f1
Sox2
Klf4
c-Myc
Esrrb
Nanog
iOSKM MEF
iPSC #1
iPSC #2
D
EB
Day 3
Day 7
Pluripotency markers
Fold mRNA expression
Pou5f1
Sox2
Day
Ectoderm
Mesoderm
Endoderm
Otx2
Twist2
Sox17

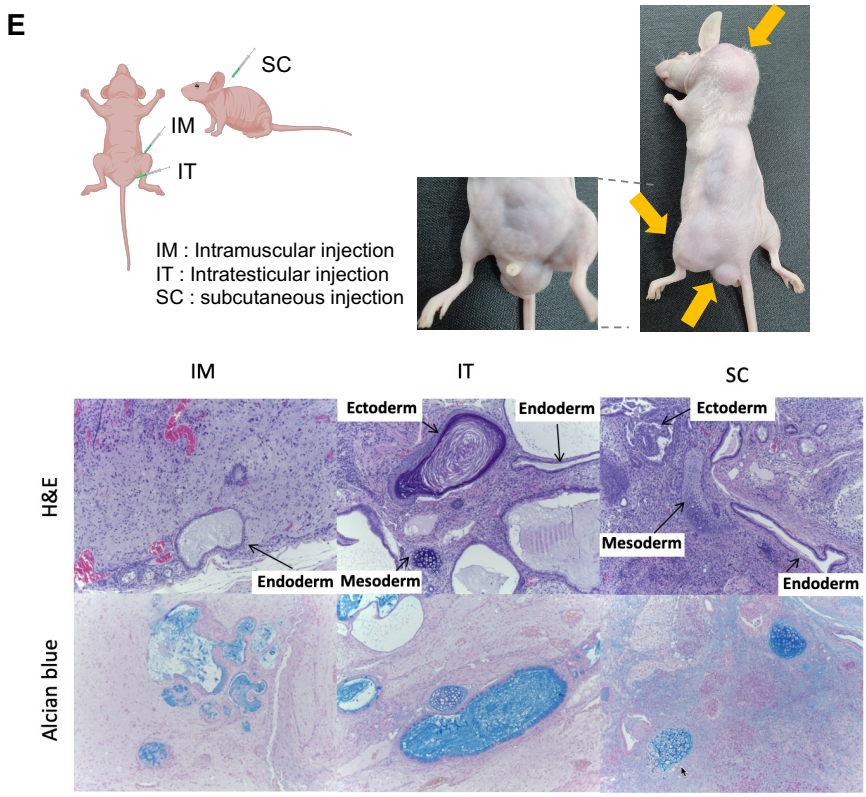

Figure 7. Generation and characterization of iPSCs derived from MEF (A) Graphical summary of i4F-MEF model. (B) Schematic view of reprogramming procedure including culture medium used. Cell clustering and iPSCs are indicated by yellow and red arrow, respectively. Images of MEF morphology changes during the stages of reprogramming. Scale bars, 200 μm. (C) Testing pluripotency of derived iPSCs by marker genes. (D) Testing pluripotency of derived iPSC by cell differentiation. (E) Testing pluripotency of derived iPSCs by teratoma formation (IM : intramuscular injection, IT : intratesticular injection, SC : subcutaneous injection).

Metabolic transition facilitates reprogramming

All mammalian cells produce ATP at different rates of glycolysis and oxidative phosphorylation (OxPHOS) (Fig. 8A). Naïve mESCs use a bivalent metabolic system that relies more on OxPHOS than primed mESCs, which exclusively use glycolysis[4, 18, 45]. Also, factors that activate glycolysis and inhibit OxPHOS promote iPSC reprogramming. To identify critical factors regulating metabolic transition during reprogramming, we energetically fractionated the MEFs population under reprogramming into ATP-high and ATP-low cell subpopulations using ATP-Red 1[40]. Figure 8B shows a schematic experimental procedure of metabolic cell fractionation with ATP- Red 1. First, we treated doxycycline (2μg/ml) in MEFs for 3days to induce early phase of reprogramming. Then, MEFs were isolated into ATP-high (top 5%) and ATP-low (bottom 5%) subpopulations by flow cytometry. We assumed that ATP low population (ATP-low) would represent the metabolic transition to glycolysis and ATP-Red 1 high population (ATP-high) would represent high OxPHOS in the middle of reprogramming. To test this hypothesis, we used Seahorse technology, which measures rate of mitochondrial oxygen flux and extracellular acidification rate. As expected, ATP-high showed higher oxygen consumption rates (OCR) than ATP-low with higher "Basal respiration" and "Maximal respiration" (Fig. 8C).

Next, we assessed reprogramming efficiency based on ATP level (Fig. 8D and E). Interestingly, ATP-low constantly revealed the higher reprogramming capacity than ATP-high (Fig. 8E).

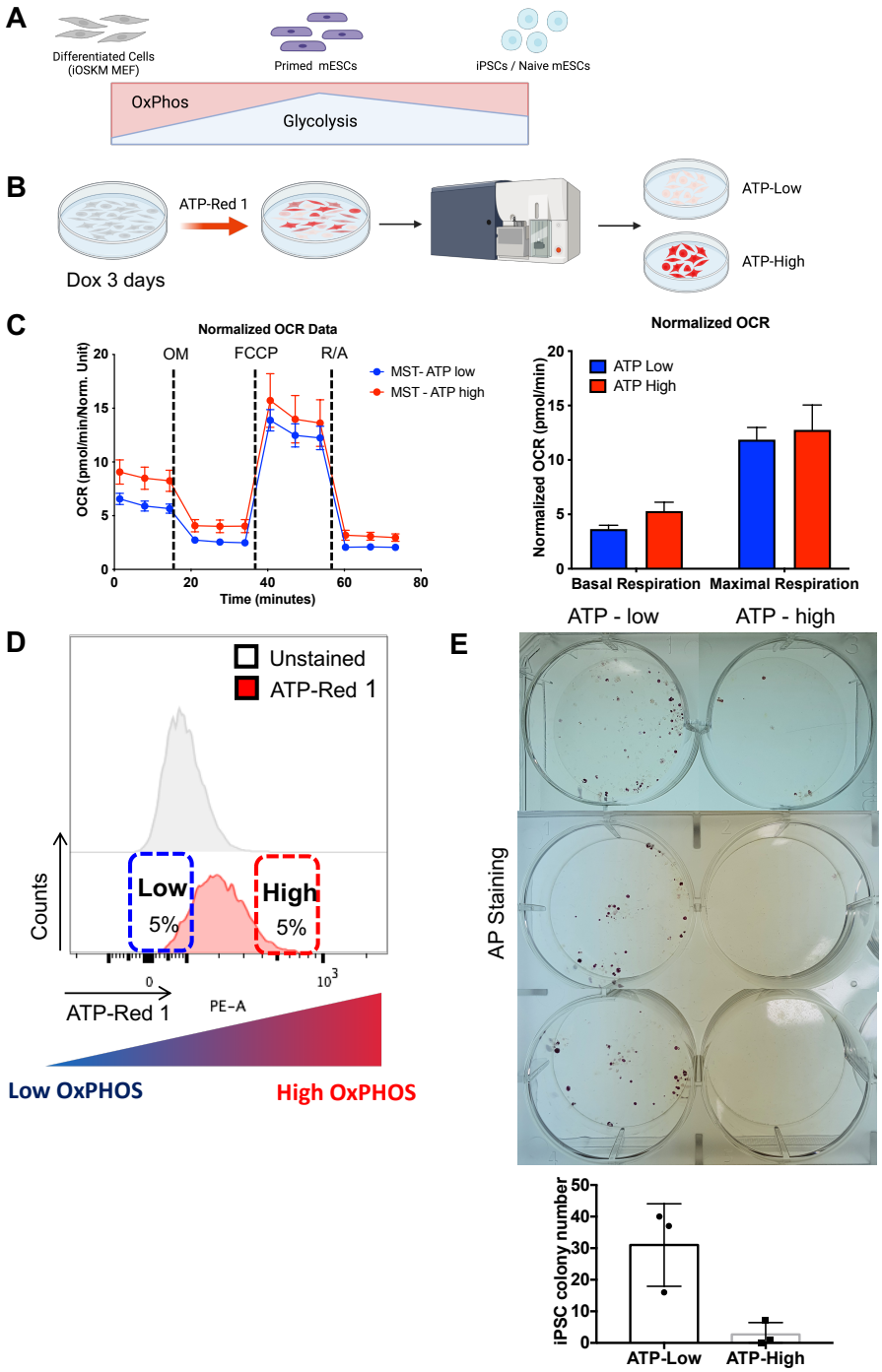

Figure 8. Higher reprogramming efficiency in ATP-low population than ATP-high population (A) Distinct metabolic features in PSCs and differentiated cells (B) Schematic view of metabolic fractionation of MEFs reprogrammed for 3 days using

ATP Red 1 (C) Oxygen consumption rates (OCR) of ATP-low and ATP-high cell subpopulations determined using the Seahorse XFe96, OM: Oligomycin, FCCP: Trifluoromethoxy carbonylcyanide phenylhydrazone, R/A: Rotenone/Antimycin-A (left panel). Indicators of OxPHOS (Basal respiration and Maximal Respiration) were measured based on assay (right panel). (D) Flowcytometric analysis of the intensity of ATP-Red1 and isolation of ATP-Red1 low/high 5% population after staining with the probe in MEFs reprogrammed for 3 days. (E) AP (alkaline phosphatse) staining of iPSC colonies obtained upon reprogramming of ATP-low and ATP-high (n = 3 independent experiments).

Upregulated EMT gene signature in ATP-high population

In order to examine the molecular mechanism, RNAseq analysis was performed to determine the molecular events. We noticed that a set of gene between ATP low and ATP high was drastically different from the parent cells, MEF. These genes turned out to be pluripotency associated gene (Fig. 9A). In this context, a set of gene in ATP low was likely to be significantly different from those of MEF compared to ATP-high (Fig. 9B). Gene ontologies of these genes included “glycolysis” and “EMT” (Fig. 9D). Further geneset enrichment analysis revealed that ATP high population is more likely to enrich epithelial gene signature (Fig. 9C).

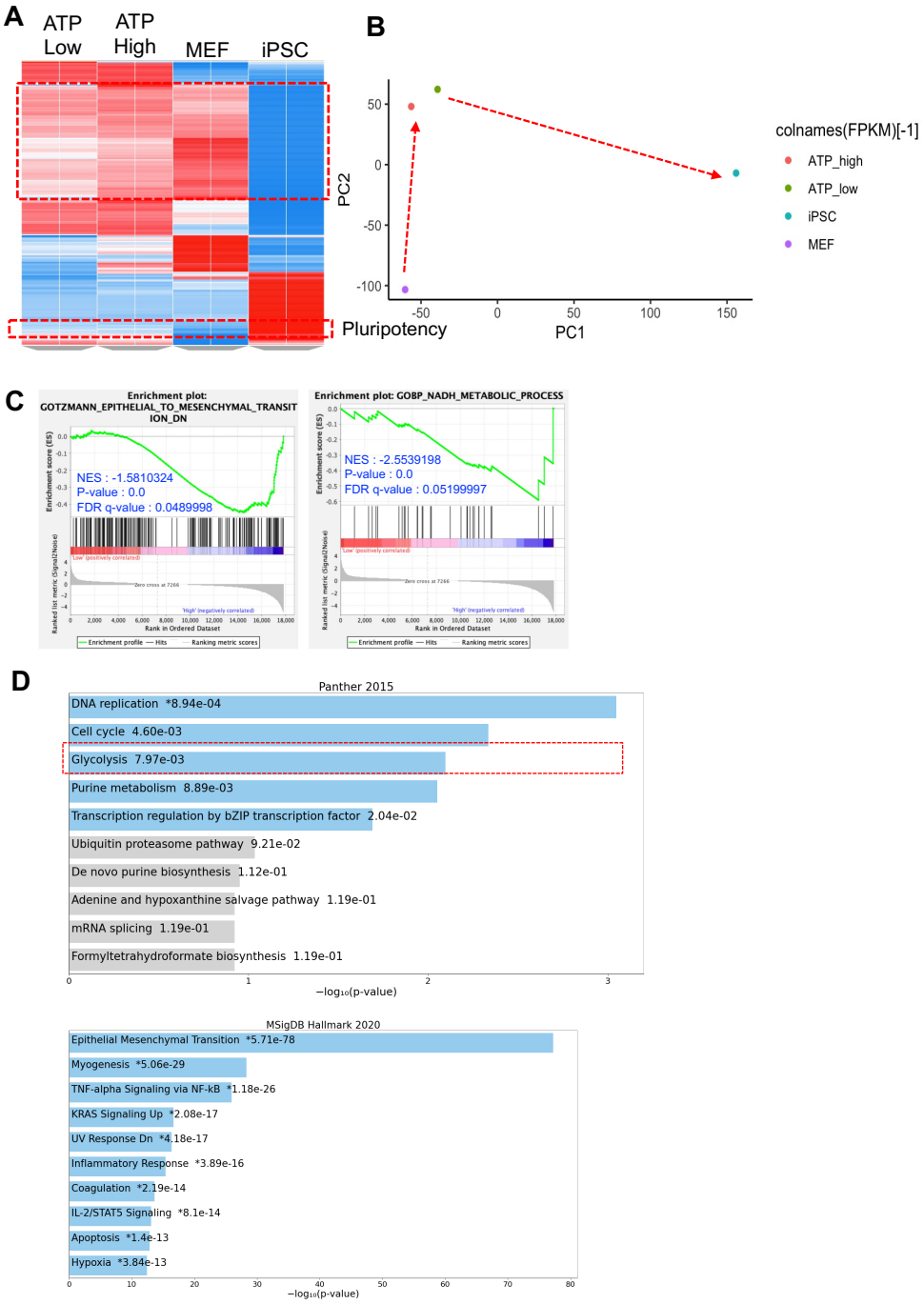

Figure 9. Upregulated EMT gene signature in ATP-high population (A) Gene expression profiles from bulk RNA-seq. (B) PCA of MEFs, ATP-low, ATP-high and iPSCs (C) Gene set enrichment Analysis between ATP-low and ATP-high cell subpopulations. (D) Gene ontologies of ATP-low and ATP-high.

Glycolysis transition is associated to MET characteristics

It is important to note that mesenchymal to epithelial transition, that is MET, is critical for efficient cellular reprogramming process, which should occur in the initial stage. Indeed, many mesenchymal genes are downregulated in MEFs at an early stage of reprogramming, which is thought to be the cause of the substantial morphological alterations associated with MET [30, 49, 50]. MET is a reverse process of epithelial-mesenchymal transition (EMT) that is vital to embryonic development.

As consistent, *Col1A1, Co1A2* and *Cdh2*, typical mesenchymal marker genes, were markedly suppressed in ATP-low population, implying that MET occurred in ATP-low population (Fig. 10A). Considering important role of Zeb2 in cellular reprogramming process [29], among typical EMT transcription factors, we determined *Zeb1* and *Zeb2* between ATP low and high population and found that *Zeb2* but not *Zeb1* was significantly suppressed in ATP-low population (Fig. 10B). This suggests a likely role for Zeb2 in metabolic transition during reprogramming. Therefore, we wondered whether *Zeb2* downregulation altered metabolic transition during reprogramming. To assess changes, we depleted the levels of Zeb2 during reprogramming using small interfering RNA (siRNA) (Fig. 10C). Of note, depletion of Zeb2 was solely sufficient to subside the level of mitochondrial ATP and activate highly expressed genes in ESCs (Fig. 10D and 10E). Also, we depleted Zeb2 level using short hairpin RNA (shRNA) lentiviral particles. Interestingly, depletion of Zeb2 facilitates the efficiency of reprogramming (Fig. 10F). These results imply that elevation of epithelial trait from i4F-MEF via Zeb2 suppression, would lead to metabolic transition for facilitating cellular reprogramming.

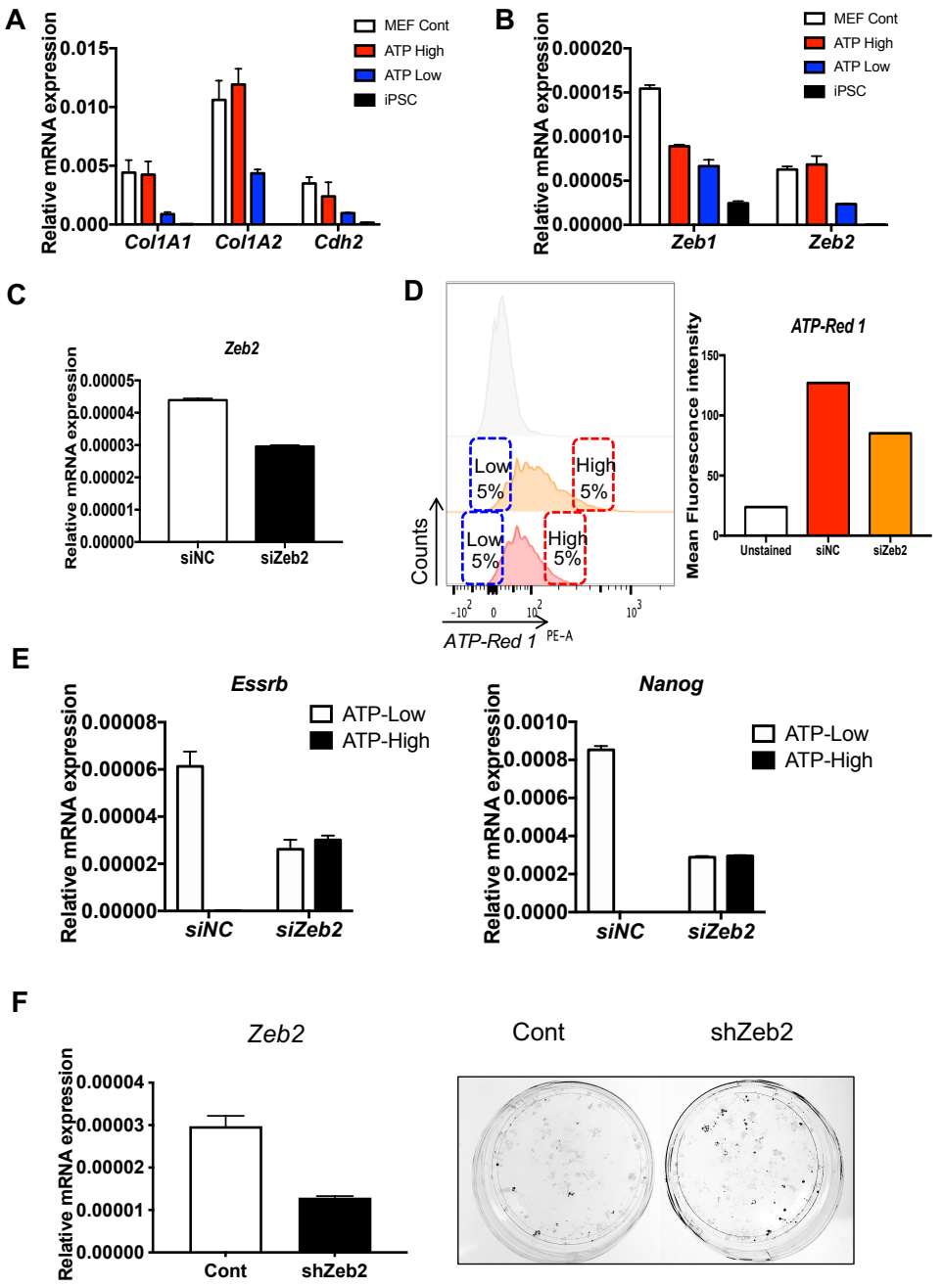

Figure 10. MET induction by Zeb2 depletion promotes reprogramming (A) Relative gene expression of EMT-related gene markers and (B) Zeb1, Zeb2 between ATP-low and ATP-high. (C) Expression of Zeb2 was downregulated following Zeb2 siRNA transfection in i4F-MEF. (D) Relative fluorescent intensity of siNC and

siZeb2 group stained with ATP-Red 1. (E) Upper and lower 5% populations of ATP-Red 1 stained cells in both siNC and siZeb2 group were isolated and reprogrammed for 15days. Relative gene expression of pluripotency markers was determined in each cell population. (F) Expression of Zeb2 was downregulated following Zeb2 shRNA transfection in i4F-MEF (left panel). Images of AP-stained colonies in control and shZeb2 (right panel).

Secondary iPSCs for reprogramming study

However, it was hard to handle MEFs since they enter senescence after a low number of passages. Thus, we expected we could handle this problem by using a secondary iPSC system [51] which regenerates iPSCs from iPSC-derived differentiated cells (Fig. 11A and 11B). We were able to observe rebound of pluripotency markers after treating doxycycline to induce reprogramming into secondary iPSCs (Fig. 11C). We validated this secondary iPSC system by removing the tumor suppressor p53, which is essential for cell cycle regulation and apoptosis [52] as it is well known that p53 deficiency increases the effectiveness of somatic cell reprogramming to a pluripotent state [53]. As expected, we could achieve higher reprogramming efficiencies in Trp53 knock-out iPSCs compared to control iPSCs (Figs 11D-F). We expect this system might be useful for understanding the role of GOI in the reprogramming process. Therefore, we are conducting experiments to obtain Zeb2 knock-out iPSCs to identify more obvious effect of Zeb2 during reprogramming.

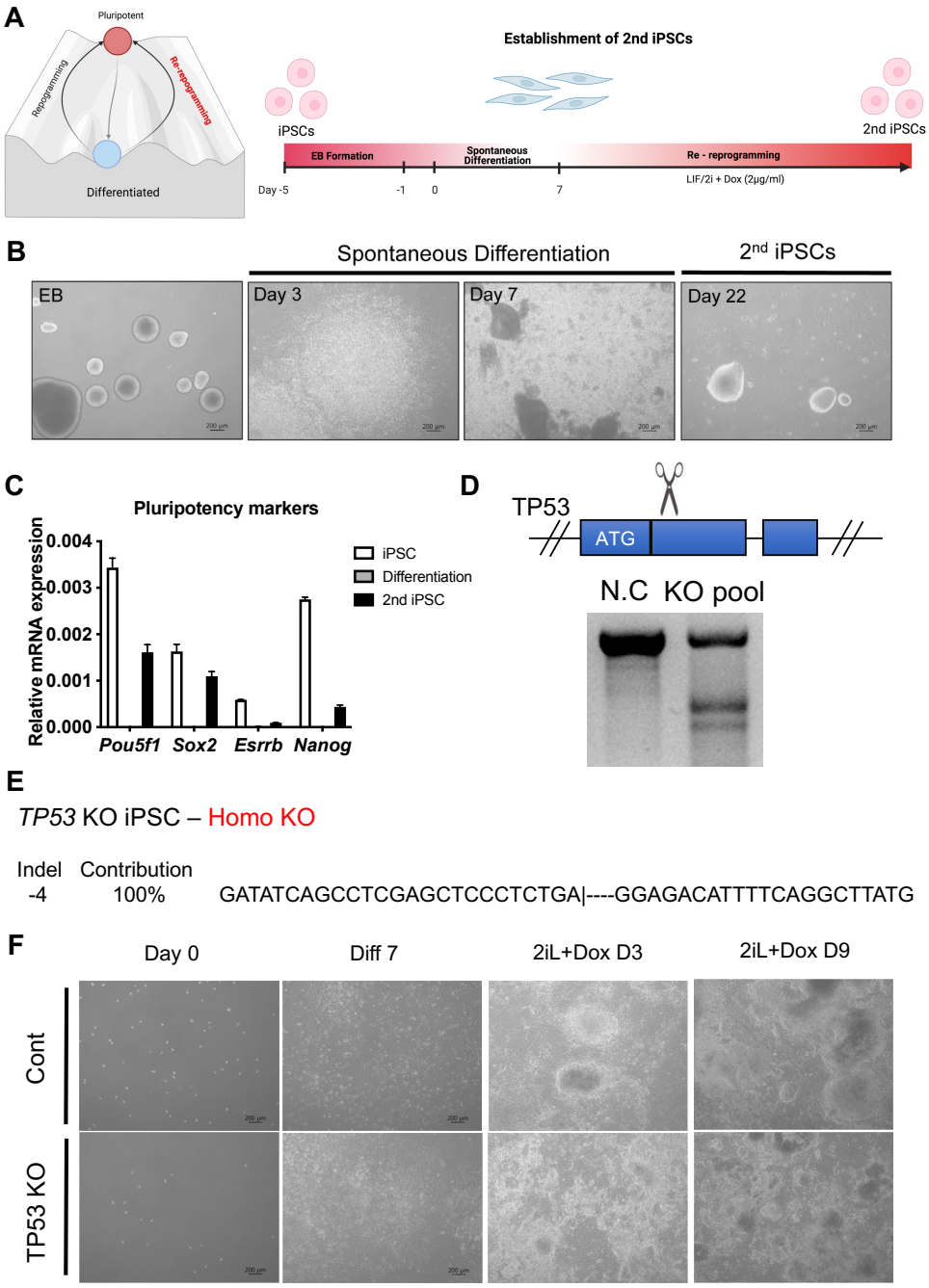

Figure 11. Generation of secondary iPSCs (A) Graphical scheme of 2nd iPSCs. (B) Representative bright field images during re-reprogramming. Scale bars, 200 μm. (C) Relative gene expression of pluripotency markers in 2nd iPSCs. (D) T7E1 assay with sgRNA of *Trp53* and Cas9 transfected iPSCs. (E) Sequence information from *Trp53*

KO iPSCs. (F) Representative bright field images during spontaneous differentiation and re-reprogramming of control and *Trp53* KO iPSCs. Scale bars, 200 μm.

Discussion

Owing to the great potential of naïve pluripotent stem cells in stem cell biology and regenerative medicine (esp., interspecies chimerism), establishing the efficient method for achieving naïve pluripotency has been intensively studied [54, 55]. To resolve the extremely low efficiency of naïve conversion, other than an efficient protocol for conversion, methodologies for live sorting or enrichment of naïve ESCs, based on surface markers of naïve ESCs [56] or the specific fluorescent probe [17], were examined.

We demonstrated that the distinct metabolic profiles of naïve compared to primed ESCs, such as high intracellular glycogen and active OxPHOS, would be strong enough to isolate or enrich the desired cell type from the mixture. High glycogen accumulation, disclosed by evident reactivity to CDg4 (Fig. 3) which resulted from the inhibition of Gsk3β followed by activation of glycogen synthase (Fig. 4) under active OxPHOS (Fig. 6), was strong enough to isolate both mouse and human naïve ESCs (Fig. 5 and Fig. 6). Additionally, the active mitochondrial respiration of naïve ESCs and high glycolysis dependence of primed ESCs (Fig. 5) enabled the enrichment of naïve ESCs by using the ATP-Red1 fluorescence probe (Fig. 6). The high stored glycogen and active OxPHOS rendered naïve ESCs to be temporally tolerant to glycolysis inhibition (Fig. 6), which readily eliminated the prime-like ESCs during naïve-to-primed conversion (Fig. 6).

It is noteworthy that glycogen accumulation following Gsk3β inhibition occurred exclusively in naïve ESCs (Fig. 2). With the gradual increase in glycogen level after fertilization until pre-implantation [25], and decrease during blastocyst development [57], glycogen is utilized as an energy source during early embryonic

development. Given that the innate ligand-receptor signaling exists to inhibit Gsk3α/β activity for naïve ESCs and pre-implantation mouse embryo [24], sustained glycogen accumulation till early blastocyst along with Gsk3β inhibition, may be necessary during embryo development, which was partly captured in these studies.

Similar to the metabolic shift from OxPHOS to glycolysis during somatic cell reprogramming to represent the biological transition [4, 21, 58], the bioenergetic remodeling to OxPHOS and subsequent glycogen accumulation would be unique traits to typify the transition to naïve pluripotency. Glycogen synthesis and storage primarily occur in the cells of the liver, skeletal muscle, and brain, and are limited in most cell types [59]. Considering a sharp contrast between the level of glycogen in naïve and primed mESCs upon iGsk3β (Fig. 2), the glycogen storage would be able to reflect the concrete metabolic shift to recapitulate a unique property of naïve pluripotency. In this regard, labeling glycogen through CDg4 or using a 2-DG or ATP-Red1 probe would be pertinent to collect naïve mESCs compared to the conventional methods based on a single surface marker [60] or a single reporter [61].

Recent studies have demonstrated that the high level of fatty acids in ESCs serves as not only an energy reservoir but also as an important determinant to maintain pluripotency through mitochondrial regulation [62]. Similarly, perturbation of fatty acid synthesis (e.g., by knockout of fatty acid synthase) or utility (e.g., by knockout of acetyl-CoA carboxylase 1) leads to massive cell death of ESCs [63] or early embryo lethality [64, 65]. As α-ketoglutarate, a metabolite product from the TCA cycle or acetyl-CoA derived from lipid oxidation determines histone modification [20, 66], a high level of glycogen or subsequent metabolic products would be important for determining naïve pluripotency in an energy-independent manner. This

interesting research subject will be explored in the future.

Recent reports have suggested that metabolic regulation is also essential and important during reprogramming, an inverse developmental path [4]. Also, it is well known that MET is an early event of cellular reprogramming and is important for acquisition of pluripotency [30]. However, the links between MET and reprogramming factors remained obscure. In this study, we have shown that downregulation of *Zeb2* may elevate the epithelial phenotype and act as a permissive trigger for subsequent MET during cellular reprogramming in MEFs. Using ATP-Red 1 probe, we were able to capture distinct metabolic profiles at an early reprogramming stage without genetic perturbation or use of small molecules and found that ATP low population showed higher reprogramming efficiency than ATP high population (Fig. 8). Our data showed that this difference might come from different EMT signature by transcriptome analysis (Fig. 9). Inhibition of Zeb2 actually altered ATP levels and increased reprogramming efficiency (Fig.10). These results suggest that ATP level based on distinct metabolic profiles can determine reprogramming efficiency. Our findings provide new insight into the relationship between metabolism and pluripotency as well as the potential of metabolic barriers in development and cellular reprogramming.

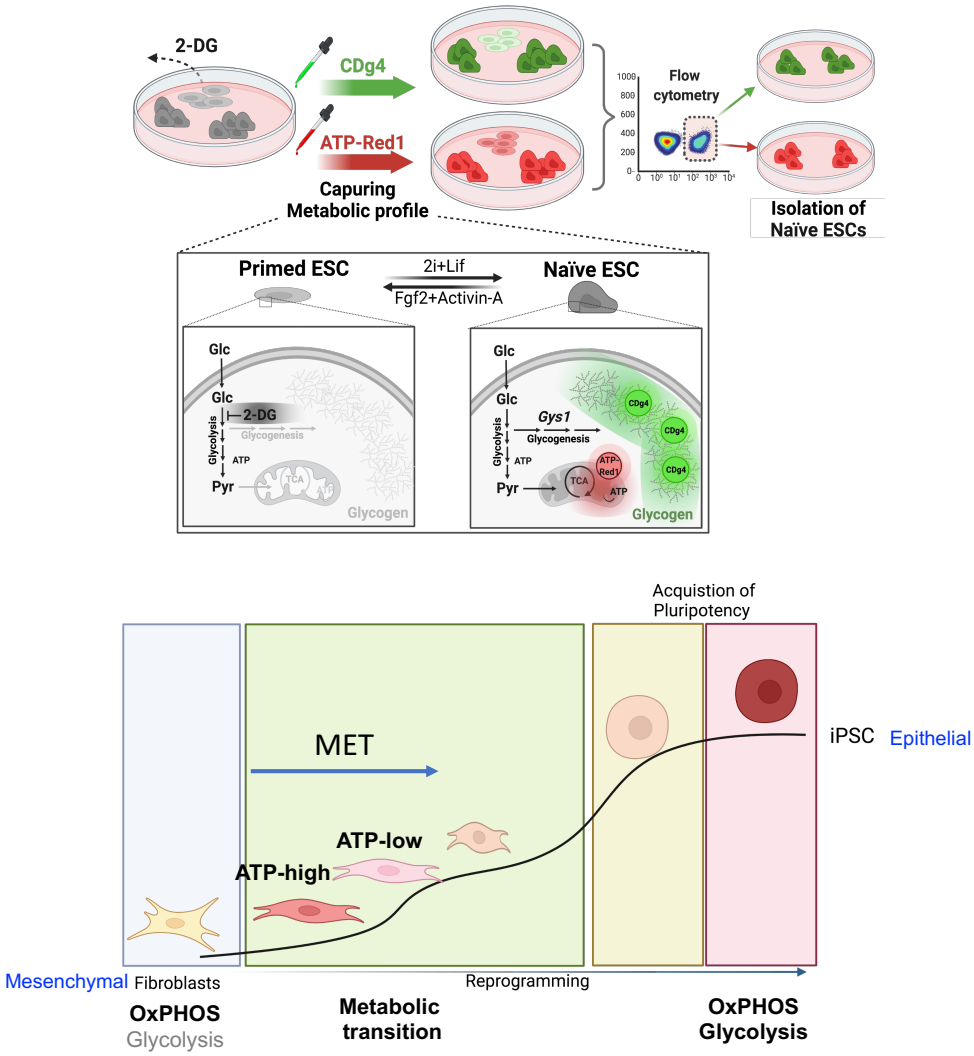

Figure 12. Graphical scheme for the study

Bibliography

1. Ginis, I., et al., *Differences between human and mouse embryonic stem cells.* Dev Biol, 2004. **269**(2): p. 360-80.
2. Shahbazi, M.N. and M. Zernicka-Goetz, *Deconstructing and reconstructing the mouse and human early embryo.* Nat Cell Biol, 2018. **20**(8): p. 878-887.
3. Nichols, J. and A. Smith, *Naive and primed pluripotent states.* Cell Stem Cell, 2009. **4**(6): p. 487-92.
4. Cha, Y., et al., *Metabolic control of primed human pluripotent stem cell fate and function by the miR-200c-SIRT2 axis.* Nat Cell Biol, 2017. **19**(5): p. 445-456.
5. Ohgushi, M., et al., *Molecular pathway and cell state responsible for dissociation-induced apoptosis in human pluripotent stem cells.* Cell Stem Cell, 2010. **7**(2): p. 225-39.
6. Kim, K.T., et al., *Safe scarless cassette-free selection of genome-edited human pluripotent stem cells using temporary drug resistance.* Biomaterials, 2020. **262**: p. 120295.
7. Jeong, H.C., et al., *PRMT8 Controls the Pluripotency and Mesodermal Fate of Human Embryonic Stem Cells By Enhancing the PI3K/AKT/SOX2 Axis.* Stem Cells, 2017. **35**(9): p. 2037-2049.
8. Cha, Y., et al., *Zap70 functions to maintain stemness of mouse embryonic stem cells by negatively regulating Jak1/Stat3/c-Myc signaling.* Stem Cells, 2010. **28**(9): p. 1476-86.
9. McLaren, A., *Sexual differentiation in mammalian chimaeras and mosaics.* Results Probl Cell Differ, 1978. **9**: p. 243-58.
10. Wu, J., et al., *Interspecies Chimerism with Mammalian Pluripotent Stem Cells.* Cell, 2017. **168**(3): p. 473-486 e15.
11. Nichols, J. and A. Smith, *Pluripotency in the embryo and in culture.* Cold Spring Harb Perspect Biol, 2012. **4**(8): p. a008128.
12. Gafni, O., et al., *Derivation of novel human ground state naive pluripotent stem cells.* Nature, 2013. **504**(7479): p. 282-6.
13. Ware, C.B., et al., *Derivation of naive human embryonic stem cells.* Proc Natl Acad Sci U S A, 2014. **111**(12): p. 4484-9.
14. Wang, J., et al., *Isolation and cultivation of naive-like human pluripotent stem cells based on HERVH expression.* Nat Protoc, 2016. **11**(2): p. 327-46.
15. Bredenkamp, N., et al., *The Cell-Surface Marker Sushi Containing Domain 2 Facilitates Establishment of Human Naive Pluripotent Stem Cells.* Stem Cell Reports, 2019. **12**(6): p. 1212-1222.
16. Collier, A.J., et al., *Comprehensive Cell Surface Protein Profiling Identifies Specific Markers of Human Naive and Primed Pluripotent States.* Cell Stem Cell, 2017. **20**(6): p. 874-890 e7.
17. Cho, S.J., et al., *A fluorescent chemical probe CDy9 selectively stains and enables the isolation of live naive mouse embryonic stem cells.* Biomaterials, 2018. **180**: p. 12-23.
18. Zhou, W., et al., *HIF1alpha induced switch from bivalent to exclusively glycolytic metabolism during ESC-to-EpiSC/hESC transition.* EMBO J, 2012. **31**(9): p. 2103-16.
19. Sperber, H., et al., *The metabolome regulates the epigenetic landscape during naive-to-primed human embryonic stem cell transition.* Nat Cell Biol, 2015. **17**(12): p. 1523-35.
20. Carey, B.W., et al., *Intracellular alpha-ketoglutarate maintains the pluripotency of embryonic stem cells.* Nature, 2015. **518**(7539): p. 413-6.

21. Zhang, J., et al., *LIN28 Regulates Stem Cell Metabolism and Conversion to Primed Pluripotency.* Cell Stem Cell, 2016. **19**(1): p. 66-80.
22. Martello, G., et al., *Esrrb is a pivotal target of the Gsk3/Tcf3 axis regulating embryonic stem cell self-renewal.* Cell Stem Cell, 2012. **11**(4): p. 491-504.
23. Sone, M., et al., *Hybrid Cellular Metabolism Coordinated by Zic3 and Esrrb Synergistically Enhances Induction of Naive Pluripotency.* Cell Metab, 2017. **25**(5): p. 1103-1117 e6.
24. Huyghe, A., et al., *Netrin-1 promotes naive pluripotency through Neo1 and Unc5b co-regulation of Wnt and MAPK signalling.* Nat Cell Biol, 2020. **22**(4): p. 389-400.
25. Stern, S. and J.D. Biggers, *Enzymatic estimation of glycogen in the cleaving mouse embryo.* J Exp Zool, 1968. **168**(1): p. 61-6.
26. Lee, S.C., et al., *Development of a fluorescent chalcone library and its application in the discovery of a mouse embryonic stem cell probe.* Chem Commun (Camb), 2012. **48**(53): p. 6681-3.
27. Takahashi, K. and S. Yamanaka, *Induction of pluripotent stem cells from mouse embryonic and adult fibroblast cultures by defined factors.* Cell, 2006. **126**(4): p. 663-76.
28. Takahashi, K., et al., *Induction of pluripotent stem cells from adult human fibroblasts by defined factors.* Cell, 2007. **131**(5): p. 861-72.
29. Wang, G., et al., *Critical regulation of miR-200/ZEB2 pathway in Oct4/Sox2-induced mesenchymal-to-epithelial transition and induced pluripotent stem cell generation.* Proc Natl Acad Sci U S A, 2013. **110**(8): p. 2858-63.
30. Li, R., et al., *A mesenchymal-to-epithelial transition initiates and is required for the nuclear reprogramming of mouse fibroblasts.* Cell Stem Cell, 2010. **7**(1): p. 51-63.
31. Polo, J.M. and K. Hochedlinger, *When fibroblasts MET iPSCs.* Cell Stem Cell, 2010. **7**(1): p. 5-6.
32. Yu, J., et al., *Induced pluripotent stem cell lines derived from human somatic cells.* Science, 2007. **318**(5858): p. 1917-20.
33. Ohnuki, M. and K. Takahashi, *Present and future challenges of induced pluripotent stem cells.* Philos Trans R Soc Lond B Biol Sci, 2015. **370**(1680): p. 20140367.
34. Haridhasapavalan, K.K., et al., *An Insight into Reprogramming Barriers to iPSC Generation.* Stem Cell Rev Rep, 2020. **16**(1): p. 56-81.
35. Kim, K.P., et al., *Permissive epigenomes endow reprogramming competence to transcriptional regulators.* Nat Chem Biol, 2021. **17**(1): p. 47-56.
36. Hong, H., et al., *Suppression of induced pluripotent stem cell generation by the p53-p21 pathway.* Nature, 2009. **460**(7259): p. 1132-5.
37. Li, H., et al., *The Ink4/Arf locus is a barrier for iPS cell reprogramming.* Nature, 2009. **460**(7259): p. 1136-9.
38. Zhu, S., et al., *Reprogramming of human primary somatic cells by OCT4 and chemical compounds.* Cell Stem Cell, 2010. **7**(6): p. 651-5.
39. Folmes, C.D., et al., *Somatic oxidative bioenergetics transitions into pluripotency-dependent glycolysis to facilitate nuclear reprogramming.* Cell Metab, 2011. **14**(2): p. 264-71.
40. Wang, L., et al., *A Multisite-Binding Switchable Fluorescent Probe for Monitoring Mitochondrial ATP Level Fluctuation in Live Cells.* Angew Chem Int Ed Engl, 2016. **55**(5): p. 1773-6.
41. Yun, S.W., et al., *Diversity oriented fluorescence library approach (DOFLA) for live cell imaging probe development.* Acc Chem Res, 2014. **47**(4): p. 1277-86.
42. Allott, L., et al., *Development of a fluorine-18 radiolabelled fluorescent chalcone: evaluated for detecting glycogen.* EJNMMI Radiopharm Chem, 2020. **5**(1): p. 17.
43. Choi, Y.K., J.J. Kim, and Y.T. Chang, *Holding-Oriented versus Gating-Oriented Live-Cell Distinction: Highlighting the Role of Transporters in Cell Imaging Probe Development.* Acc Chem Res, 2019. **52**(11): p. 3097-3107.
44. Ying, Q.L., et al., *The ground state of embryonic stem cell self-renewal.* Nature,

2008. **453**(7194): p. 519-23.
45. Zhang, J., et al., *Metabolism in Pluripotent Stem Cells and Early Mammalian Development.* Cell Metab, 2018. **27**(2): p. 332-338.
46. Kim, K.T., et al., *Live isolation of naive ESCs via distinct glucose metabolism and stored glycogen.* Metab Eng, 2022. **72**: p. 97-106.
47. Carey, B.W., et al., *Single-gene transgenic mouse strains for reprogramming adult somatic cells.* Nat Methods, 2010. **7**(1): p. 56-9.
48. Hochedlinger, K., et al., *Ectopic expression of Oct-4 blocks progenitor-cell differentiation and causes dysplasia in epithelial tissues.* Cell, 2005. **121**(3): p. 465-77.
49. Samavarchi-Tehrani, P., et al., *Functional genomics reveals a BMP-driven mesenchymal-to-epithelial transition in the initiation of somatic cell reprogramming.* Cell Stem Cell, 2010. **7**(1): p. 64-77.
50. Stadtfeld, M., et al., *Defining molecular cornerstones during fibroblast to iPS cell reprogramming in mouse.* Cell Stem Cell, 2008. **2**(3): p. 230-40.
51. Banito, A. and J. Gil, *Induced pluripotent stem cells and senescence: learning the biology to improve the technology.* EMBO Rep, 2010. **11**(5): p. 353-9.
52. Levine, A.J. and M. Oren, *The first 30 years of p53: growing ever more complex.* Nat Rev Cancer, 2009. **9**(10): p. 749-58.
53. Banito, A., et al., *Senescence impairs successful reprogramming to pluripotent stem cells.* Genes Dev, 2009. **23**(18): p. 2134-9.
54. Weinberger, L., et al., *Dynamic stem cell states: naive to primed pluripotency in rodents and humans.* Nat Rev Mol Cell Biol, 2016. **17**(3): p. 155-69.
55. Ying, Q.L. and A. Smith, *The Art of Capturing Pluripotency: Creating the Right Culture.* Stem Cell Reports, 2017. **8**(6): p. 1457-1464.
56. Collier, A.J., et al., *Comprehensive Cell Surface Protein Profiling Identifies Specific Markers of Human Naive and Primed Pluripotent States.* Cell Stem Cell, 2017.
57. Thomson, J.L. and R.L. Brinster, *Glycogen content of preimplantation mouse embryos.* Anat Rec, 1966. **155**(1): p. 97-102.
58. Panopoulos, A.D., et al., *The metabolome of induced pluripotent stem cells reveals metabolic changes occurring in somatic cell reprogramming.* Cell Res, 2012. **22**(1): p. 168-77.
59. Adeva-Andany, M.M., et al., *Glycogen metabolism in humans.* BBA Clin, 2016. **5**: p. 85-100.
60. Bi, Y., et al., *Identification of ALPPL2 as a Naive Pluripotent State-Specific Surface Protein Essential for Human Naive Pluripotency Regulation.* Cell Rep, 2020. **30**(11): p. 3917-3931 e5.
61. Choi, H.W., et al., *Distinct Enhancer Activity of Oct4 in Naive and Primed Mouse Pluripotency.* Stem Cell Reports, 2016. **7**(5): p. 911-926.
62. Wang, L., et al., *Fatty acid synthesis is critical for stem cell pluripotency via promoting mitochondrial fission.* EMBO J, 2017. **36**(10): p. 1330-1347.
63. Tanosaki, S., et al., *Fatty Acid Synthesis Is Indispensable for Survival of Human Pluripotent Stem Cells.* iScience, 2020. **23**(9): p. 101535.
64. Chirala, S.S., et al., *Fatty acid synthesis is essential in embryonic development: fatty acid synthase null mutants and most of the heterozygotes die in utero.* Proc Natl Acad Sci U S A, 2003. **100**(11): p. 6358-63.
65. Abu-Elheiga, L., et al., *Mutant mice lacking acetyl-CoA carboxylase 1 are embryonically lethal.* Proc Natl Acad Sci U S A, 2005. **102**(34): p. 12011-6.
66. McDonnell, E., et al., *Lipids Reprogram Metabolism to Become a Major Carbon Source for Histone Acetylation.* Cell Rep, 2016. **17**(6): p. 1463-1472.

국 문 초 록

세포 역분화(cellular reprogramming) 시 일어나는 해당과정으로의 대사 전환(metabolic transition)은 유전자 저해(Gene perturbation) 후 효율을 확인함으로써 다능성(Pluripotency)을 획득하기 위한 전제 조건인 것으로 입증되었다. 이 연구에서 본인은 미토콘드리아 ATP 특이적 형광 프로브인 ATP-Red 1과 유도성 역분화 인자를 포함하는 생쥐 배아 섬유아세포(mouse embryonic fibroblast) [i4F-MEF]를 사용하여 역분화로 유도된 대사 전환 집단을 실시간으로 얻어 특성 분석을 수행하였다. 역분화 중간 과정에서 실시간으로 얻은 해당 과정으로의 대사 전환을 나타내는 ATP-Red 1 low (ATP-low) 집단은 ATP-Red 1 high (ATP-high) 집단보다 일관되게 더 높은 역분화 능력을 나타냈다. ATP-low 집단과 ATP-high 집단 사이의 전사체 프로파일 분석(Transcriptome profile analysis)을 통해 우리는 ATP-low 집단의 전사체가 상피-간엽이행(epithelial-mesenchymal transition, EMT)의 핵심 조절자인 Zeb2(Zinc finger E-box-binding homeobox 2)의 명확한 억제 양상을 보이며 EMT와 음의 상관 관계가 있음을 입증했다. 흥미롭게도, Zeb2의 녹다운(Knock-down)은 미토콘드리아의 ATP 수준을 낮추었으며, 역분화 효율을 향상시키는 데 충분하였다. 이러한 결과는 Zeb2 억제를 통한 i4F-MEF의 상피(epithelial) 특성 상승이 세포 역분화를 촉진하기 위한 대사 전환으로 이어질 것임을 암시한다.

주요어: Zeb2, Reprogramming, EMT(상피간엽이행), Metabolic transition(대사전환), ATP-Red 1, iPSC

학번: 2020-20464

Acknowledgements

인턴으로 실험실 들어온 지가 엊그제 같은데, 벌써 제가 졸업을 할 시기가 되었네요. 지난 2년 반 동안의 여정을 되새겨 보니, 대학원에서 보낸 시간은 제 인생에서 가장 행복하고 찬란한 시간이었습니다. 제가 이렇게 즐거운 대학원 생활을 할 수 있었던 건 모두 좋은 교수님과 실험실 사람들 덕분이라고 생각합니다. 도움을 주신 모든 분들께 감사의 말을 전하고 싶습니다.

가장 먼저, 학위 과정 동안 아낌없는 지도를 해주신 차혁진 교수님께 깊은 감사의 말씀을 드립니다. 학부 때 교수님의 열정적인 수업을 듣고 감명받았었는데, 대학원에서 교수님의 연구에 대한 열정에 또 한번 깊은 감명을 받았습니다. 저에게 잠재된 역량을 이끌어내고자 좋은 피드백과 많은 기회를 주셔서 정말 감사했습니다. 앞으로 교수님께 배운 것들을 머리와 마음에 새기고 주체적인 연구자로서 열심히 살아가겠습니다.

Naïve 팀의 수장이자 저의 사수였던 근태 오빠, 항상 친절히 가르쳐 주시고, 망했다고 생각한 실험에서도 의미를 찾아 주셨을 정도로 배려심 넘치는 오빠 덕분에 늘 힘과 용기를 얻었습니다. 또한, 실험실의 어떤 일에도 항상 자기 일처럼 도와 주시는 모습을 보면서 오빠처럼 좋은 선배, 좋은 사람이 되고 싶다는 생각을 늘 했어요. 소울메이트 주미 언니, 실행력과 연구에 대한 열정이 넘치는 언니에게 in vivo 실험을 배울 수 있어서 영광이었어요. 제가 걱정이 많은 편인데 항상 언니가 저의 모든 걱정을 지워 주셔서 덕분에 항상 든든했습니다. 졸업 메이트 영현 오빠, 박사 졸업을 축하드려요! 실험하다가 모르는 게 생기면 오빠에게 자주 조언을 구했는데, 그때마다 친절하게 답변해주시고 함께 고민해 주셔서

감사했습니다. 척척박사라는 말이 잘 어울리는 주찬 오빠, 항상 창의적인 아이디어를 내고 그것을 실현해내는 오빠를 보며 멋있다고 생각했어요. 게다가 밤낮, 주말 없이 열심히 하시는 모습을 보며 많은 자극이 되었습니다. 다정한 민정 언니, 석사 과정과 분야가 많이 다름에도 빠르게 적응하시는 언니를 보며 대단하다고 느꼈어요. 항상 따뜻하게 잘 챙겨 주셔서 감사했어요. 멋진 선배이자 친구인 윤정이, 프로페셔널하게 실험하는 윤정이를 보며 좋은 자극이 되었어. 그리고 처음에 웨스턴블랏 과정 익히느라 진땀 뺄 때 웨스턴 요정 윤정이가 도와준 덕에 잘 익힐 수 있었어. 고마워. 귀여운 동생이자 멋진 선배인 성민이, 연구에 대한 열정이 뛰어난 너를 보며 많이 배웠어. 같은 Naïve 팀이라 너에게 의지를 많이 했던 것 같아. 정말 잘하는 너니까 앞으로 Naïve 팀을 잘 이끌어 나갈 수 있을 거야. 화이팅! 분위기 메이커 승연 언니, 처음에 연구실 들어와 함께 실험 배울 때 똑똑한 승연 언니 덕분에 더 잘 이해할 수 있었어. 항상 용기 북 돋아주고, 잘 챙겨줘서 고마워. 쾌활한 은지, 항상 밝은 에너지로 기운을 주고, 걱정과 고민도 진지하게 들어주었던 은지 덕분에 행복했어. 실험도 꼼꼼하게 잘 알려주고, 긍정적인 영향을 많이 줘서 정말 고마워. 승연 언니와 은지, 둘 덕분에 연구실에 빨리 적응할 수 있었고, 즐겁고 재밌는 실험실 생활을 했어. 둘 다 너무 고맙고, 특히 함께 얘기하면서 컵라면 먹던 시간이 그리울 것 같아. 듬직한 범기, 팁 같이 꼽고 in vivo 실험 함께하면서 빨리 친해졌었지. 평소에는 유쾌하고 연구할 땐 진지한 범기를 보며 정말 배울 점이 많았어. 옆자리였던 동우, 이야기도 잘 들어주고 뭐든 친절하게 알려줘서 고마웠어. 연구 주제도 잘 찾아가는 것 같아 대견해. 유쾌한 다연이, 다정하게 잘 대해줘서 고마웠어. 분야가 달라서 많이 못 도와준

것 같은데, 언제든 궁금한 것 있으면 편하게 연락해. 다음 학기부터 들어올 따뜻한 윤제, 진지한 연준이, 열정 넘치는 태주, 바쁘다는 핑계로 더 많이 챙겨주지 못해서 미안해. 너희들의 시작을 응원할게. 그리고 항상 열심히 공부하시던 석우 오빠, 다정하고 멋진 선배였던 정윤이를 포함해 졸업하신 모든 실험실 선배님들께도 감사의 마음을 전하고 싶습니다.

마지막으로 항상 저에게 큰 힘이 되어주시는 사랑하는 가족에게도 감사를 전합니다. 제가 어떤 일을 하든 따뜻한 마음으로 응원해주시는 아빠, 매일 매일 제 이야기를 들어주시고 저를 위해 기도해주셨던 엄마, 항상 저를 아껴주시는 할머니 그리고 의지가 되는 오빠, 언니 모두 감사드립니다.

2022 년 7 월

오지영 올림